RICE UNVIERSITY

Poly(NIPAAm-co-AAm)-gold nanoshell composites for optically-triggered cancer therapeutic delivery

by

Laura Elizabeth Strong

A THESIS SUBMITTED
IN PARTIAL FULFILLMENT OF THE
REQUIREMENTS FOR THE DEGREE

Master of Science

APPROVED, THESIS COMMITTEE:

Jennifer L. West, PhD. (Chair)
Isabel C. Cameron Professor of
Bioengineering

Rebekah A. Drezek, PhD.
Professor of Bioengineering and Electrical &
Computer Engineering

Sibani L. Biswal, PhD.
Assistant Professor of Chemical and
Biomolecular Engineering

HOUSTON, TX
DECEMBER 2012

ABSTRACT

Poly(NIPAAm-co-AAm)-gold nanoshell composites for optically-triggered cancer therapeutic delivery

by

Laura Elizabeth Strong

Cancer is currently the second leading cause of death in the United States. Although many treatment options exist, some of the most common, including radiotherapy and chemotherapy, are restricted by dose-limiting toxicities. For example, for 2-6% of patients receiving a regimen of the chemotherapeutic doxorubicin, irreversible cardiotoxicity will occur[1], causing these patients to immediately cease treatment. In addition, the largest hurdle for translating novel biological therapies such as siRNA into the clinic is lack of an efficient delivery mechanism to get the therapeutic into malignant cells[2]. Both of these situations would benefit from a minimally invasive controlled release system that only delivers a therapeutic to the site of malignant tissue. This thesis presents work towards the creation of such a delivery platform using two novel material components: a thermally responsive poly[N-isopropylacrylamide-co-acrylamide] (NIPAAm-co-AAm) hydrogel and gold-silica nanoshells. Thermally responsive hydrogels go through a physical property transition at their lower critical solution temperature (LCST). When transitioning from below to above the LCST, the hydrogel material expels large amounts of water and absorbed molecules. This phase change can be optically triggered by embedded gold-silica nanoshells, which rapidly transfer near-infrared (NIR) light energy into heat energy due to the surface plasmon resonance phenomena. When this material is loaded with absorbed drug molecules, drug release can be externally triggered by exposure to an NIR laser.

Initial characterization of this material was done using bulk hydrogel-nanoshell composites. Poly(NIPAAm-co-AAm)-nanoshell composites were synthesized via free radical polymerization. The LCST of the poly(NIPAAm-co-AAm) hydrogels was determined to be from 39-45 ^{o}C, or slightly above physiologic temperature. The material was swollen in a drug solution of either doxorubicin (a common chemotherapeutic) or a 21bp dsDNA olgio (a

model molecule for siRNA). Composites were then exposed to an 808 nm laser at 8 W/cm^2, which was found to trigger release of the therapeutics from the composite material.

Further work has been done in translating this composite material to nano-scale sized particles, such that it could be injected intravenously and passively accumulate in tumor tissue. Sub-micron composite particles were synthesized using dissolvable gelatin templates with 500 nm wells. Analysis by transmission electron microscopy (TEM) shows that these particles consist of gold nanoshells surrounded by a hydrogel coating. Analysis by dynamic light scattering (DLS) shows that these particles display the same thermal properties as seen in the bulk material, collapsing in response to increased temperatures and NIR light exposure. Ultimately, the work in this thesis advances the development of a minimally-invasive, optically-triggered drug delivery platform.

Acknowledgements

I would like to acknowledge and thank all the members of the West Lab for their advice and support, especially those members of the nanoshell team: Dr. Emily Day and Andy Coughlin. I would also like to thank Dr. Melissa McHale and Dr. Maude Cuchiara for her help with edits and revisions. I would like to thanks Dr. Ryan Schweller for helpful discussions about DNA and siRNA as well as his assistance with PAGE. Funding sources include the Nanobiology Interdisiplinary Graduate Training Program (NIH Grant No. T32EB009379) and the HHMI Med Into Grad Training Program.

Table of Contents

List of Figures

List of Tables

1 INTRODUCTION: CANCER BIOLOGY, CLINICAL MANAGEMENT, AND CONTROLLED DRUG DELIVERY

1.1 MOTIVATION

In 2010, cancer was the second leading cause of death in the United States following heart diseases, accounting for approximately 1500 deaths/day[3]. In addition, over the past 15+ years, the death rate due to heart disease rate has decreased 40%, while the cancer death rate has only been reduced by 18% as seen in Figure 1.1[3]. Furthermore, the cost of cancer was estimated to be $263.8 billion annually[3]. These statistics indicate that advances in cancer treatments are still needed in order to better manage this disease. The work in this thesis aims to improve cancer treatment by utilizing a novel platform to better control the delivery of cancer therapeutics.

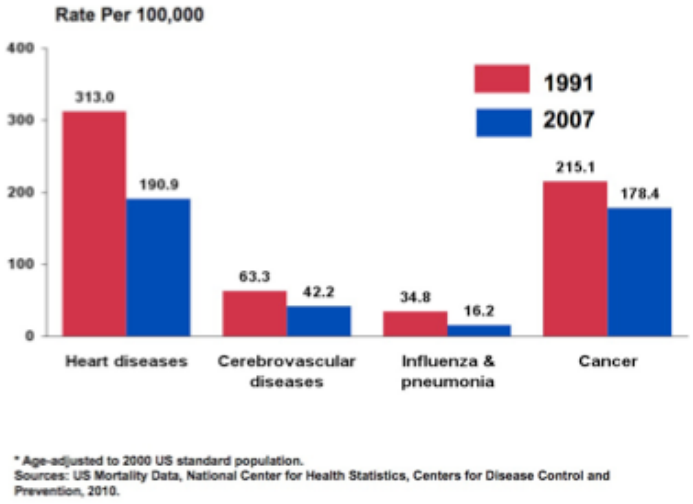

Figure 1.1. US mortality rates for several diseases in 1991 and 2007. Information age adjusted to 2000 US standard population. From Ref 3.

1.2 CANCER HALLMARKS

Cancer is widely recognized to be a disease involving dynamic changes in the genome. It occurs in a wide variety of cell types and tissues but is universally characterized

by cell changes that allow for unregulated cell cycle progression and growth. Tumorigenesis is a multistep process in which each step reflects genetic alterations that drive a progressive transformation of normal cells into highly malignant derivatives[4]. In a 2000 review, Hanahan and Weinburg assert that this transformation into a malignant state manifests in six essential alterations in cell physiology: (1) self-sufficiency in growth signals, (2) insensitivity to growth-inhibitory (anti-growth) signals, (3) limitless replicative potential, (4) evasion of programmed cell death (apoptosis), (5) sustained angiogenesis, and (6) tissue invasion and metastasis[4]. The authors note that these capabilities are shared in common by most, if not all types of human tumors.

Over the past 10 years, progress in cancer research has led to new observations that serve to both clarify and modify the original six hallmarks. In response, Hanahan and Weinburg wrote another review in 2011, in which four new concepts were discussed[5]. Two of these new concepts, (1) genome instability and mutation and (2) tumor-promoting inflammation, are thought be critical to the scope and conceptualization of the original six hallmarks. In addition, two new, unique hallmarks were recognized: (1) reprogramming of energy metabolism and (2) evading immune destruction.

1.3 CANCER THERAPY

Conventional cancer treatments include surgery, radiation therapy, and chemotherapy. These treatments may be used alone but are often used in combination. The goal of each treatment option is to kill as much malignant tissue as possible while minimizing harm to surrounding healthy tissues.

Surgical therapy involves the physical removal (resection) of the tumor mass. This is the most effective treatment for localized disease. It is common for adjacent, healthy tissue to be resected during surgery to help pathologists determine if the tumor is invading surrounding tissue and decrease the risk of recurrence or metastasis. However, surgery is not applicable for tumors in inaccessible anatomic locations or in cases with extensive intermingling of tumor and critical normal tissues[6].

In radiation therapy, tumor cells are exposed to ionizing radiation resulting in cell death when the cell tries to divide. Therefore, this therapy is most toxic to highly proliferative cells, including cancer cells. However, both malignant cells and healthy tissue use the same mechanism for cell division, and thus, radiation therapy also kills rapidly dividing normal cells within renewing tissues such as hair follicles, oral-gastrointestinal epithelium, and hematopoietic tissue. These off-site toxicities, along with other chronic toxicities, ultimately determine the maximum dose of radiation a patient may receive in his or her lifetime[6].

Chemotherapy is defined as the use of drugs to treat or control cancer. These drugs are often given systemically and aim to target highly proliferative cells. These types of drugs include alkylating agents, antimetabolites, natural or semisynthetic products, and hormones or hormone inhibitors[7]. The drugs are generally cell cycle phase-specific, as demonstrated in Figure 1.2, and thereby target highly proliferative cells to a greater degree than more dormant tissues[8].

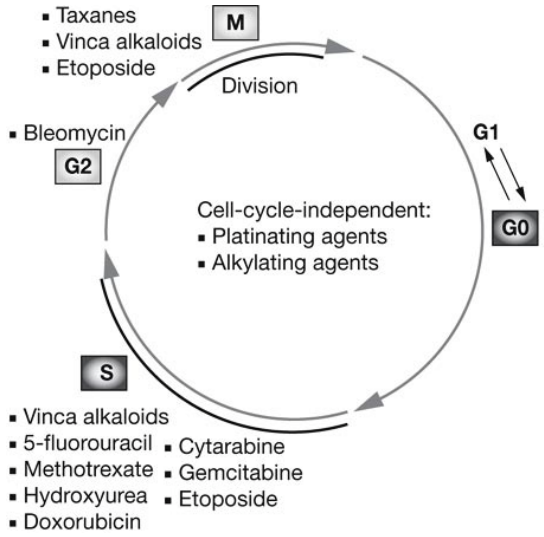

Figure 1.2. Cell cycle schematic and respective sensitivity to chemotherapeutic agents. Most agents are active in the S and M phases of the cell cycle and thereby target more proliferative tissues to a higher degree than more dormant tissues Adapted from Seiwert *et al.* 2007[8].

Like radiation therapy, off-site toxicities of chemotherapeutics are significant in tissues that are normally in a highly proliferative state, such as the bone marrow, gastrointestinal tract, and hair follicles[7]. This leads to the side effects that most people associate with chemotherapy regimens: immunosuppression, nausea, and alopecia. However, many chemotherapeutics also have less common toxic reactions, including pulmonary fibrosis (seen with bleomycin, buslfan, and mitocycin C) and cardiotoxicity (seen with doxorubicin, daunomycin, mitoxantrone, and idarubicin)[7]. These severe toxicities often lead to restrictions in the total doses of these drugs that may be administered[7]. If a patient experiences one of these toxicities, treatment often has to be ceased immediately, even if the drug is effective against the malignant cells. These drugs would benefit from administration in a manner that minimizes drug exposure to healthy tissues. A more detailed explanation of controlled drug delivery can be found in Section 1.3.2.

1.3.1 Emerging Therapy: siRNA

In recent years, advancing technologies in molecular biology have demonstrated that small segments of RNA can be used as a genetics-based cancer therapy. In RNA interference, double stranded RNA (dsRNA) hinders the expression of a target gene as a result of sequence homology[2]. This process occurs naturally in mammalian cells, where the enzyme Dicer initiates RNA silencing by breaking down long dsRNA molecules into small interfering RNA (siRNA) segments of around 21-23 nucleotides[2]. The siRNA molecules go on to bind to complementary sequences in cytosolic mRNA transcripts, thereby preventing protein translation of the binding targets. The overall process of RNA interference is summarized in Figure 1.3[9].

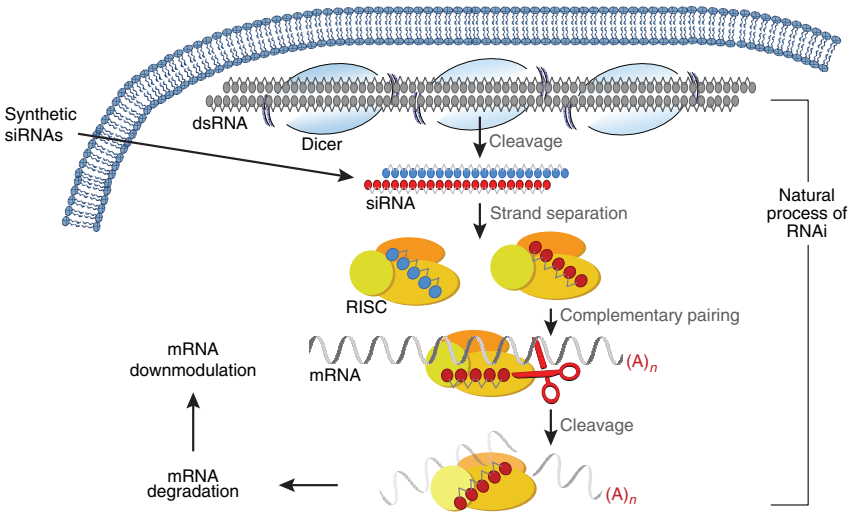

Figure 1.3 Cellular mechanisms of RNA interference. First, dsRNA is cleaved by Dicer into siRNA. These siRNAs are then incorporated into the RNA-induced silencing complex (RISC), where the strands are separated. The RISC complex containing the antisense strand seeks out to bind to complementary mRNA sequences. These mRNA sequences are than cleaved by the enzyme Argonaute, thereby causing mRNA degradation and preventing protein translation. From Bumcrot *et al.* 2006[9].

This biological mechanism can be exploited for cancer therapy by the introduction of synthetic siRNA targeted to a gene of choice. Elbashir *et al.* first showed that the introduction of a 21-nucleotide artificial siRNA could trigger gene silencing in mammalian cells[10]. This proof of concept study demonstrated the downregulation of several different genes coding for various firefly luciferases[10]. Since then, siRNA has been used to downregulate key proteins in the progression of cancer showing great therapeutic potential. As a result, siRNA has been investigated for use in the treatment of cancers of the breast, ovary, cervix, liver, lung, prostate, and others[2]. Furthermore, several siRNA molecules have advanced to human clinical trials, as shown in Table 1.1.

Table 1.1. siRNA Therapeutics in Clinical Trials. From Oh *et al.* 2009[2].

Companies	Product	Target gene	Target disease	Route of administration	Status
Opko Health	Bevasiranib (Cand 5)	VEGF	AMD	Intravitreal	Phase III
			DME		Phase II
Allergan	AGN211745 (Sirna-027)	VEGF receptor	AMD	Intravitreal	Phase II
Alnylam Pharmaceuticals	ALN-RSV01	RSV	RSV infection	Intranasal	Phase II
Quark Pharmaceuticals	RTP801i-14	RTP801	AMD	Intravitreal	Phase I
	AKIi-5	p53	ARF	Intravenous	Phase I
Calando Pharmaceuticals	CALAA-01	M2 subunit of ribonucleotide reductase	Solid tumor	Intravenous	Phase I
Nucleonics	NUC B1000	HBV	`HBV infection	Intravenous	Phase I
TransDerm	TD101	Single nucleotide mutation in the keratin 6a	PC	Intradermal	Phase I

VEGF: Vascular endothelial growth factor, DME: Diabetic macular edema, RSV: respiratory syncytial virus, AMD: age-related macular degeneration, HBV: Hepatitis B virus, ARF: Acute renal failure, PC: Pachyonychia congenital.

siRNA therapy has several advantages over more traditional therapeutic strategies. First, siRNA interferes with translation, not with DNA transcription as seen in DNA-based gene therapy approaches. Therefore, this approach minimizes concerns about possible adverse gene alterations[2]. Another advantage is that siRNA can act on a wide range of protein targets, whereas traditional chemical drugs are limited to acting on certain classes of receptors, ion channels, or enzymes. Current biological therapies, including monoclonal antibodies and cytokines, mainly target moieties on the cell surface. siRNAs, however, can target any mRNA regardless of the cellular location of the translated protein[2].

A major challenge in the translation of siRNA therapy to the clinic is the efficient delivery of the molecule into target cells[2]. RNA is anionic and hydrophilic and therefore cannot enter cells by passive diffusion. In addition, RNA molecules injected intravenously are quickly degraded by serum enzymes and cleared rapidly through the kidneys[9]. Furthermore, these molecules have limited penetration across capillary endothelium and inefficient uptake by parenchymal cells[9]. Development of an *in vivo* delivery system for siRNA is paramount for an efficient therapeutic effect to take place[2].

1.3.2 Controlled Delivery Methods

Therapeutic efficacy of both chemotherapeutics and biological therapeutics such as siRNA would benefit from administration in a controlled delivery manner. Controlled delivery systems can influence the performance of a therapeutic agent by manipulation of its effective concentration, location, and duration[11]. Drug delivery via controlled release offers several advantages to improve cancer therapy including (1) localized delivery of the drug to a particular tissue, thereby lowering the systemic drug level, (2) preservation of drugs that are rapidly broken down by the body, (3) reduced need for follow-up care, (4) increased comfort, and (5) improved compliance[12].

The field of controlled drug release has grown dramatically from the 1940s when sustained release products aiming to reduce the frequency of dosing first came on the market. Today a wide range of self-regulating systems deliver a variety of molecules including genes, proteins, and other therapeutics[11]. In fact, in a review dating back to 1981, Langer and Peppas noted that while synthesis and discovery of new potent drugs is important, critical attention should also be given to the manner in which these drugs are delivered[13]. Current

research in cancer medicine also focuses on the synthesis and discovery of new and effective drugs. In fact, Hanahan and Weinburg described several drugs that aim to interfere with each of the acquired hallmarks of cancer in their recent review (Figure 1.4)[5].

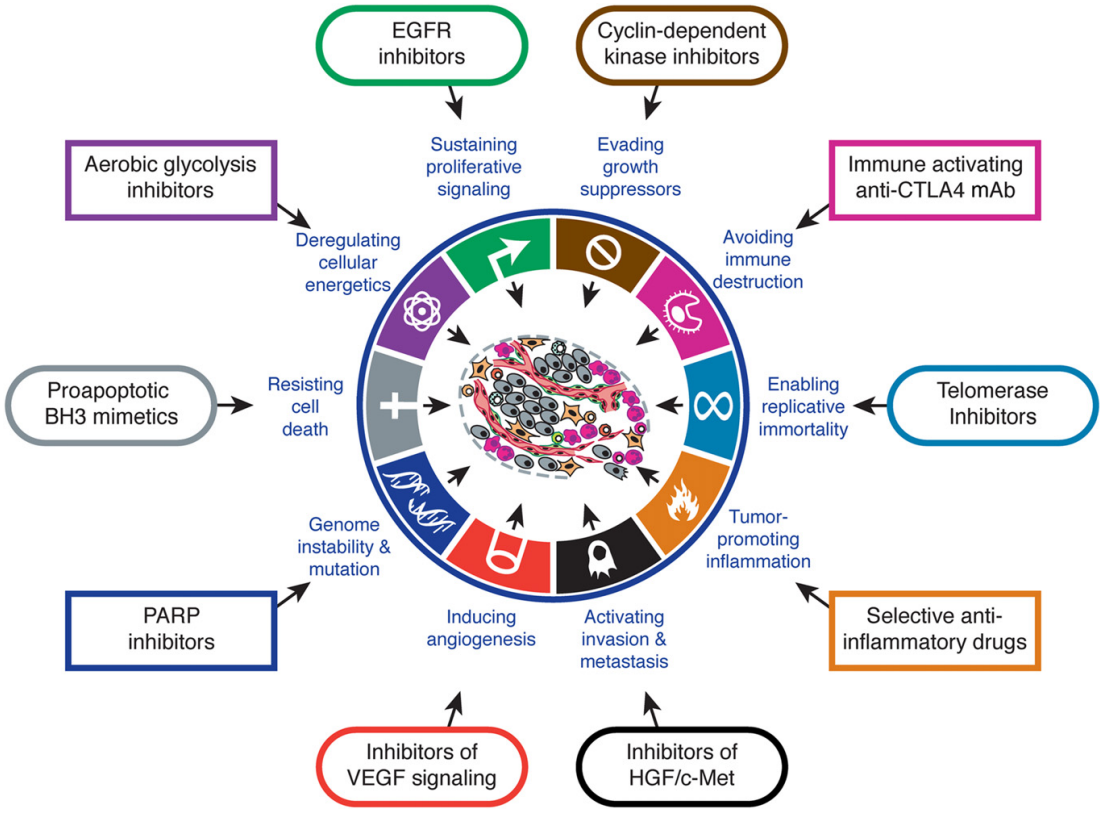

Figure 1.4. Therapeutic targeting of the ten hallmarks of cancer. Drugs that interfere with each acquired capability of cancer cells listed are either in clinical trials or approved for clinical use in certain forms of cancer. From Hanahan and Weinburg 2011[5].

In addition to this focus on novel drugs, new methods of delivery should also be investigated. The chemotherapeutic off-site toxicities mentioned previously, which tend to be responsible for failed or aborted chemotherapy regimens, could be minimized by use of a controlled delivery system. This system would provide burst drug delivery only to malignant tissue, effectively minimizing drug exposure to non-malignant tissues.

There are some controlled delivery systems on the market today, most notably Doxil®, which is a poly(ethylene glycol) [PEGylated] liposome containing the chemotherapeutic doxorubicin[14]. This formulation increases the serum half-life of the drug, thereby ensuring a higher percentage of the administered dose reaches the tumor site[14]. However, Doxil® is given systemically and some drug will diffuse out of the liposome over time, leading to off-site toxicity.

Another commercially available delivery system is bis-chloronitrosourea (BCNU) wafers (Gliadel®) for the management of brain malignancies. This therapy consists of polifeprosan 20 wafers loaded with the chemotherapeutic Carmustine. These wafers are implanted directly into the brain during surgical tumor resection, and slowly release drug over time to prevent recurrence[15]. However, surgical access is necessary for implantation making this strategy inapplicable for some cancer sites. A non-invasive drug delivery system that allows drug release to occur only at the tumor site would be advantageous over existing drug delivery systems.

1.4 CONCLUSIONS

The systems discussed in this section are not without their limitations. A non-invasive platform, which can be externally triggered to release a therapeutic only at the site of malignant tissue, would be an improvement in cancer management. This thesis investigates such a system. This platform will be comprised of two novel material components: gold-silica nanoshells and a thermally responsive polymer coating. The polymer coating would contain drug, allowing the drug-filled particles to circulate throughout the body without the drug acting on tissue. At the appropriate delivery site, the optical properties of the gold-silica

nanoshells would be exploited to increase the particle temperature and trigger drug release. A background on these two material components follows in Chapter 2.

2 MATERIAL COMPONENTS[1]

2.1 INTRODUCTION

The work in this thesis involves two unique materials: a gold-based nanoparticle and a thermally responsive hydrogel. This chapter provides background information on these two materials as well as examines previous studies of these materials in relation to cancer management and drug delivery. The chapter concludes with combinations of these two materials as well as remarks regarding current limitations.

2.2 GOLD NANOPARTICLES

Nanoparticles have been highly investigated for use in biological and medical applications due to their unique size and optical properties. The four main gold nanoparticle types that will be further discussed are solid gold nanoparticles (AuNPs), gold-gold sulfide (Au-Au_2S) nanoparticles, gold-silica (SiO_2-Au) nanoshells, and gold nanorods. All of these particles are of importance in biomedical applications because of their ability to induce localized heating upon exposure to light. Additional properties of these particles are summarized in Table 2.1.

[1] Portions of this chapter have been adapted from the publication: L.E. Strong and J.L. West. "Thermally Responsive Polymer-Nanoparticle Composites for Biomedical Applications." *Wiley interdisciplinary reviews. Nanomedicine and nanobiotechnology*. 2011;3(3):307-17.

Table 2.1. Nanoparticle Properties[16–20].

Au Nanoparticles	Au-Au_2S Nanoparticles	Silica-Au Nanoshells	Au Nanorods
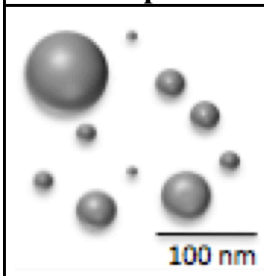	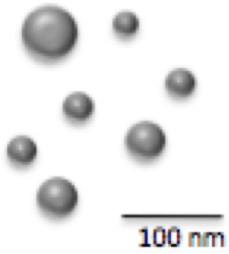	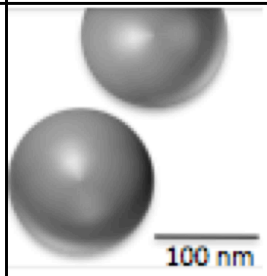	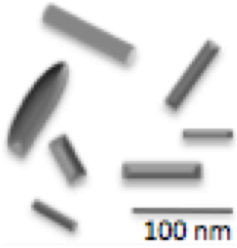
Diameter: 2-100 nm	**Diameter:** 30-40 nm	**Diameter**: 120-150 nm	**Aspect Ratio:** 1.5-10 (ex: 20x100 nm)
Extinction: 520-575 nm	**Extinction** (tunable): ~850 nm	**Extinction** (tunable): ~800 nm	**Extinction**: 600-1300 nm
Pros: highly investigated, ease of synthesis	**Pros:** NIR absorbance	**Pros:** NIR absorbance	**Pros:** NIR absorbance
Cons: extiniction coefficent near that of hemoglobin	**Cons:** synthesis byproduct of gold colloid	**Cons**: large	**Cons:** surfactant toxicity from synthesis

2.2.1 Optical Properties

When a gold-based nanoparticle is irradiated with light at the wavelength of its surface plasmon resonance, this light is rapidly transferred into thermal energy, causing a localized temperature increase[16–18]. Au-Au_2S nanoparticles, Silica-Au nanoshells, and Au nanorods can all be tuned to have a surface plasmon resonance in the near infrared (NIR) range[17–20]. The NIR range (700-900 nm) is above the absorption of biological molecules such as hemoglobin (<650 nm) and below the range absorbed by water (>900 nm)[21]. Thus, NIR light is of particular interest for biological applications, as these wavelengths penetrate biological tissue with relatively little attenuation or tissue damage, as illustrated in Figure 2.1[21].

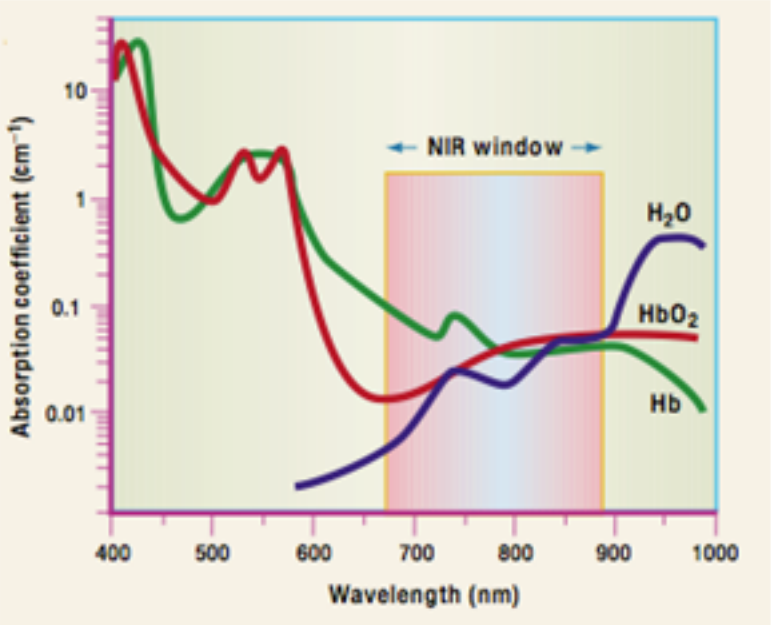

Figure 2.1. Tissue permeability of NIR light. Near-infrared light (650-900 nm) is of particular interest in biological applications as it is minimally absorbed by biological chromophores and water. From Weissleder 2001[21].

2.2.2 Types of Gold Nanoparticles

Gold nanoparticles (AuNPs, also called gold colloids) are one of the most stable and highly investigated metal nanoparticle[16]. These particles, thought of as "soluble gold" in antiquity, were used for aesthetic and curative purposes as early as the 4th and 5th centuries B.C[16]. Several synthesis techniques exist, the most common being citrate reduction of chloroauric acid ($HAuCl_4$) in water[22]. These particles (with diameters ranging from 2-100 nm) have maximum absorption around 520-575 nm, depending on the diameter of the particles, with the smaller particles maximally absorbing at a lower wavelength[16].

2.2.2.1 Gold-gold sulfide nanoparticles

Gold-gold sulfide (Au-Au_2S) nanoparticles were first developed by Zhou *et al.*[23]. Due to their optical properties, these particles were originally thought to consist of a dielectric gold-silica core surrounded by a thin gold shell[18]. Controversy still remains over the exact structure of these particles; however the core/shell model fits the optical data and surface conjugation studies suggest a continuous gold coating[24]. These nanoparticles are synthesized by mixing $HAuCl_4$ and sodium sulfide (Na_2S)[23]. The ratios of these two materials can be adjusted to alter the surface plasmon resonance of the particles from 600 nm to greater than 1000 nm[25]. Much research has been done on Au-Au_2S nanoparticles that are NIR absorbing; these particles generally have a 35-55 nm diameter and surface plasmon resonance near 800-900 nm[18,26–30].

2.2.2.2 Gold-silica nanoshells

Gold-silica nanoshells were developed by Oldenburg *et al.* through molecular self-assembly and colloid reduction chemistry[31]. These particles consist of a dielectric silica core surrounded by a solid gold shell, and adjustments of these two parameters provide control over the optical properties of the particles, as seen in Figure 2.2[19]. The peak extinction coefficients of these particles can range from visible to near-infrared and even infrared ranges[19]. Most photothermal studies have utilized particles with a 120 nm core and 10 nm shell, as this corresponds to a peak absorption coefficient in the near infrared range, where biological tissue is most permissive to light[19,28,32–36].

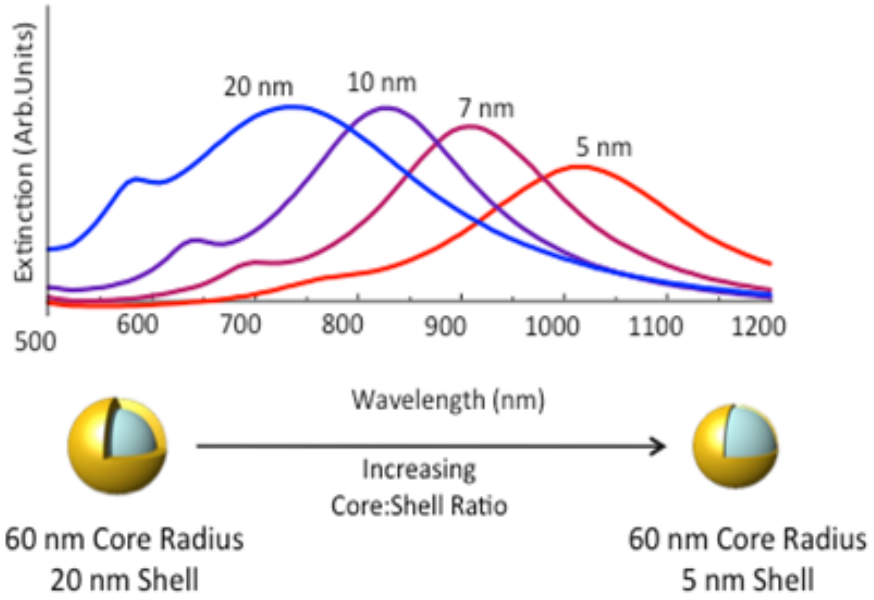

Figure 2.2. Optical tunability of gold-silica nanoshells. By altering gold-silica core:shell ratios, optical tunability can be obtained. A thinner shell causes a red shift in absorbance. Adapted from Hirsch *et al* 2006[19].

2.2.2.3 Gold Nanorods

Gold nanorods are anisotropic nanoparticles composed of solid gold, where particle shape strongly influences optical properties. Gold nanorods show a surface plasmon band near 520 nm similar to spherical AuNPs, but also have a second band at a longer wavelength[37]. These optical properties are much more dependent on the particle's aspect ratio (ratio of length to diameter)[20]. The dominant surface plasmon band occurs at a longer wavelength, and is based on the axial length of the particle[20]. The secondary surface plasmon band occurs around 520 nm due to the weaker transverse resonance[20]. Particles with larger aspect ratios will have the primary longitudinal resonance at a longer wavelength than

particles with a smaller aspect ratio[20]. These particles can be synthesized either by use of rigid templates or, more commonly, by use of seed and growth solutions in the presence of surfactants[38].

2.2.3 Gold Nanoparticles in Cancer Medicine

Near infrared absorbing gold nanoparticles, particularly gold-silica nanoshells, have been investigated for both imaging and therapy applications in cancer medicine. This is due to numerous advantageous properties of the particles. First, the outer shell of these particles is made of reduced gold, a material known to be biocompatible due to its resistance to corrosion and low toxicity[19]. Second, the size of these particles allows them to be injected intravenously and passively accumulate in tumor tissue due to the enhanced permeability and retention (EPR) effect[39]. This phenomenon is observed mainly due to four unique characteristics of tumor growth: (1) architectural defects, (2) high vascular density, (3) impaired lymphatic drainage, and (4) generation of permeability enhancing factors[40]. Finally, the optical extinction of nanoshells involves both scattering and absorption components. The scattering properties of nanoshells can be harnessed for optical imaging of the particles using dark field microscopy, optical coherence tomography (OCT), or reflectance confocal microscopy (RCM)[26,27]. In addition, when these particles absorb light, the electron-photon interactions within the gold shell yield to heat dissipation and result in photothermal ablation of nearby cancer cells[19]. Photothermal therapy is advantageous for cancer management as cell death only occurs where both nanoshell accumulation and NIR light exposure occur, minimizing off-site toxicity commonly seen in other cancer treatment modalities.

2.2.3.1 *in vitro* studies

Photothermal therapy using gold-silica nanoshells was first demonstrated by Hirsch *et al.* in 2003[41]. In this study, SK-BR-3 human breast carcinoma cells were incubated with gold-silica nanoshells and exposed to an NIR laser (820 nm, 35 W/cm^2). Results, shown in Figure 2.3, show the cells incubated with nanoshells die upon NIR exposure, whereas cells without nanoshells retain their viability after irradiation by an NIR laser[41].

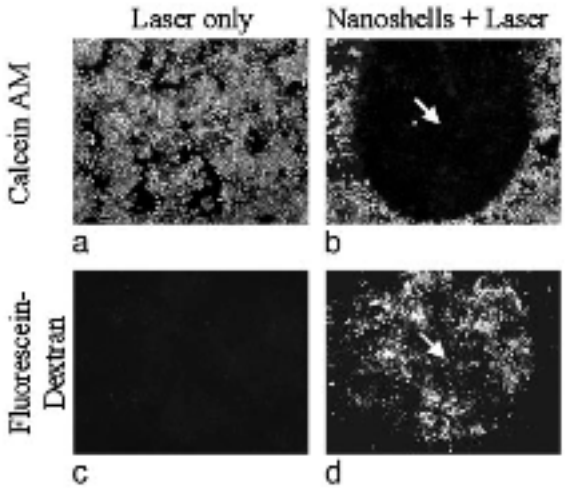

Figure 2.3. *In vitro* validation of photothermal therapy. Cells irradiated in the absence of nanoshells maintain both viability as determined by Calcein AM staining (A) and membrane integrity as demonstrated by a lack of dextran uptake (C). Cells irradiated in the presence of nanoshells shown a circular zone of cell death in the Calcein AM image (B) and increased membrane permeability as demonstrated by an uptake in fluorescent dextran (D). From Hirsch *et al.* 2003[41].

Subsequent *in vitro* studies have focused on active targeting of nanoshells using antibodies and other protein based ligands including anti-HER2[26,42,43], anti-IL13Rα2[43], and ephrinA1[44]. Gold-gold sulfide nanoparticles have also been investigated for photothermal therapy potential *in vitro*, displaying similar results as gold-silica nanoparticles[24,45].

2.2.3.2 *in vivo* studies

Photothermal therapy has been further evaluated in several *in vivo* studies, most commonly in mouse models. In the first study by Hirsch *et al.*, transmissible venereal tumor (TVT) cells were inoculated in the hind leg of SCID mice and grown to a diameter of ~1cm[41]. Poly(ethylene glycol) (PEG)-passivated gold silica nanoshells were injected interstitially at the tumor site. Nanoshells are often coated with polymer chains such as PEG as this has been shown to minimize plasma protein adsorption and therefore increase *in vivo* circulation time of the particles. Next, tumor sites were exposed to 820 nm light at 4 W/cm^2, while temperature profiles were obtained using phase-sensitive, fast spoiled gradient-echo MRI. Results showed an average temperature increase of 9.1±4.7 ^{o}C, and gross pathology, as shown in Figure 2.4, showed tissue damage and hemorrhaging.

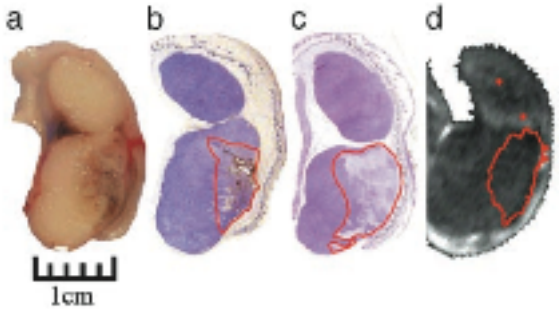

Figure 2.4. Gross histology after photothermal ablation. (A) Gross pathology indicates hemorrhaging and loss of tissue birefringence. (B) Silver staining of a tissue section exposes region of localized nanoshells (outlined in red). (C) Hematoxylin/eosin staining reveals tissue damage within the area occupied by nanoshells. (D) Calculations from MR images further indicate an area of irreversible thermal damage. From Hirsch *et al.* 2003[41].

Not all tumor sites are amenable to the direct injection of particles into the tumor. Recent studies have shown the ability of gold-silica nanoshells to be injected intravenously, circulate throughout the body, and accumulate in tumor tissue via the EPR effect. In the first

of such studies by O'Neal *et al.*, PEGylated gold-silica nanoshells were injected into the tail vein of mice with a subcutaneous tumor[46]. The tumor was exposed to a 808 nm diode laser 6 hours post-injection. In addition, a "sham" group received a saline injection followed by laser treatment, and a control group received no treatment. Figure 2.5 shows a Kaplan-Meyer survival plot for the three groups. All mice that received nanoshell-assisted photothermal therapy (NAPT) survived for the 60 day period, whereas the mean survival for the control and sham groups were 10.1 days and 12.5 days respectively. Additional *in vivo* studies have shown the potential for nanoshells to be used as both imaging contrast agents for OCT and particles for photothermal therapy simultaneously[27], as well as a potential treatment for malignant glioma[47]. In addition, gold-gold sulfide particles have also been investigated for *in vivo* photothermal therapy[24].

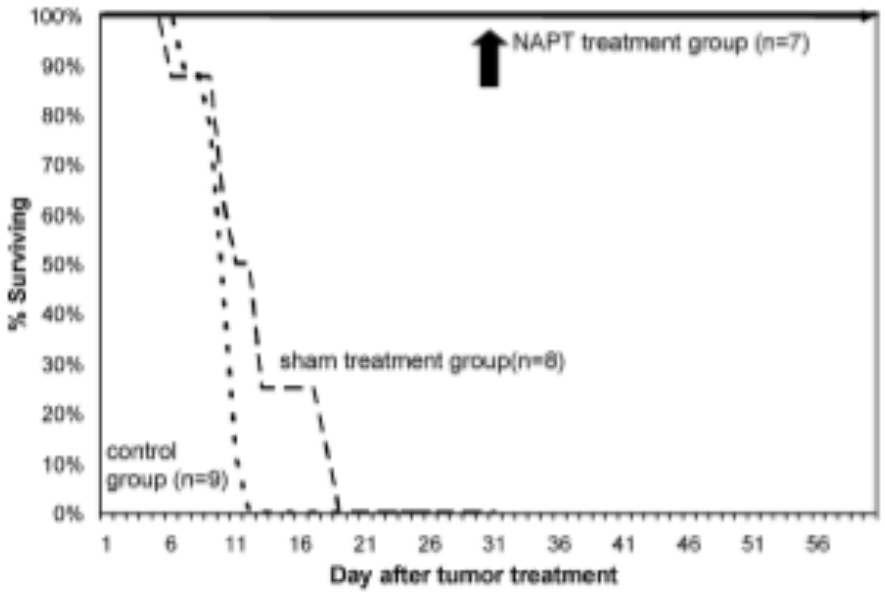

Figure 2.5 Survival curve for NAPT. NAPT mice showed 100% survival after 60 days, while the sham and control groups had an average survival of 12.5 and 10.1 days respectively. From O'Neal *et al.* 2004[46].

Studies of the biodistribution and clearance of gold-silica nanoshells indicate that the particles are primarily cleared via the liver and spleen[48]. Figure 2.6 shows the biodistribution of nanoshells at 24 hours post injection, indicating much higher concentrations in the tumor versus most other tissues.

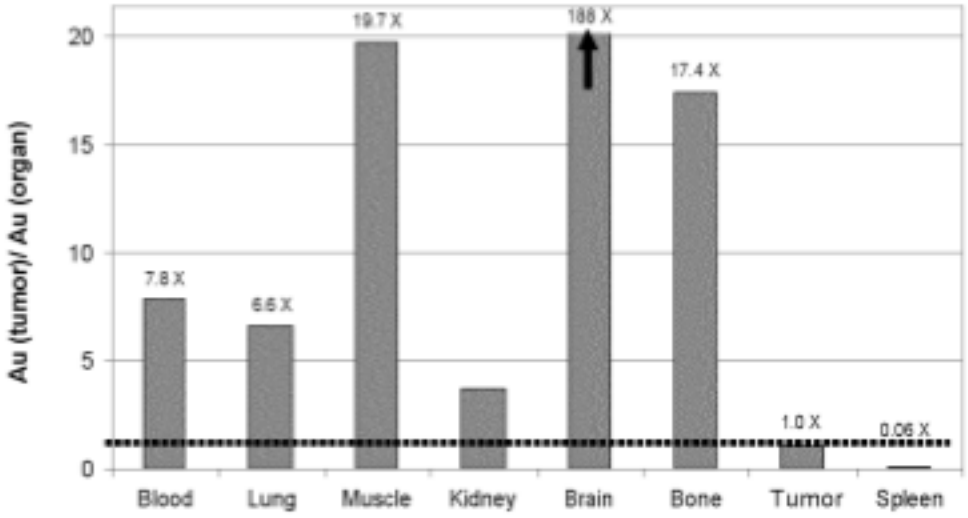

Figure 2.6. Biodistribution of gold nanoshells. Shown are ratios of gold concentration in various tissues to that of tumor at 24 hours post nanoshell injection. Tumor tissue displays significantly more gold content than all organs excluding the spleen. From James *et al.* 2007[48].

Due to the promise shown in these *in vivo* studies, photothermal therapy with gold-silica nanoshells is currently in FDA clinical trials for refractory head and neck cancer[49]. In this treatment, nanoshells are injected to the patient, allowed to passively accumulate in the tumor, and then the tumor site is exposed to NIR light from a fiber optic probe[49].

2.3 THERMALLY RESPONSIVE POLYMERS

The gold-silica nanoshells previously described will provide the stimulus for drug release from a polymer coating. Stimuli-responsive 'smart' polymers undergo fast, reversible

conformational changes in response to small changes in the environment[50]. Changes in the polymer's conformation usually involve the polymer microstructure transitioning between a hydrophilic and hydrophobic state and result in macroscopic material size and properties change as well[50]. Systems responsive to local chemical changes, such as changes in pH, as well as systems responsive to external stimuli, such as ultrasound, light, or temperature, have been studied[51]. Temperature-sensitive systems are easy to synthesize and control, making them suitable for many applications[51]. Commonly studied temperature-sensitive polymers include acrylamide-based hydrogels, especially poly[N-isopropylacrylamide] (PNIPAAm), as well as elastin-like polypeptides (ELPs)[50–53].

At a temperature-sensitive polymer's lower critical solution temperature (LCST), a reversible volume phase transition occurs. At lower temperatures, it is thermodynamically favorable for water molecules to form hydrogen bonds with polar groups on the polymer chains, causing the hydrogel to be in its swollen state. At higher temperatures, there is an increase in Gibbs free energy (ΔG), and hydrogen bonding between the water molecules and polymer chains becomes thermodynamically unfavorable compared to polymer-polymer and water-water interactions[54]. This causes the water to move into bulk solution and the polymer chains to collapse onto themselves forming hydrophobic interactions[55]. A common property characterized in thermally responsive systems is the polymer's deswelling ratio (DSR), a measurement of the degree of collapse a hydrogel undergoes at its LCST.

2.3.1 N-isopropylacrylamide and other acrylamides

Poly[N-isopropylacrylamide] (PNIPAAm) is a widely studied thermally-responsive polymer that exhibits an LCST near physiologic temperatures[51]. Pure PNIPAAm hydrogels

have an LCST range of 25-32^{o}C, and by incorporating a more hydrophilic comonomer into the hydrogel, this LCST can be raised to near 45-50^{o}C[56]. Common comonomers used include acrylamide (AAm) or acrylic acid (AAc), with a 95:5 molar ratio of NIPAAm:AAm resulting in a gel with an LCST of approximately 40^{o}C[29]. In addition, incorporation of N-isopropylmethacrylamide (NIPMAAm) increases the LCST as steric hindrance by the additional methyl group inhibits the phase transition[57]. In contrast, hydrogels consisting of hydrophilic acrylamide/acrylic acid monomers exhibit a positive volume change with increasing temperatures[58,59]. A summary of the chemical structures of various acrylamides can be found in Figure 2.7.

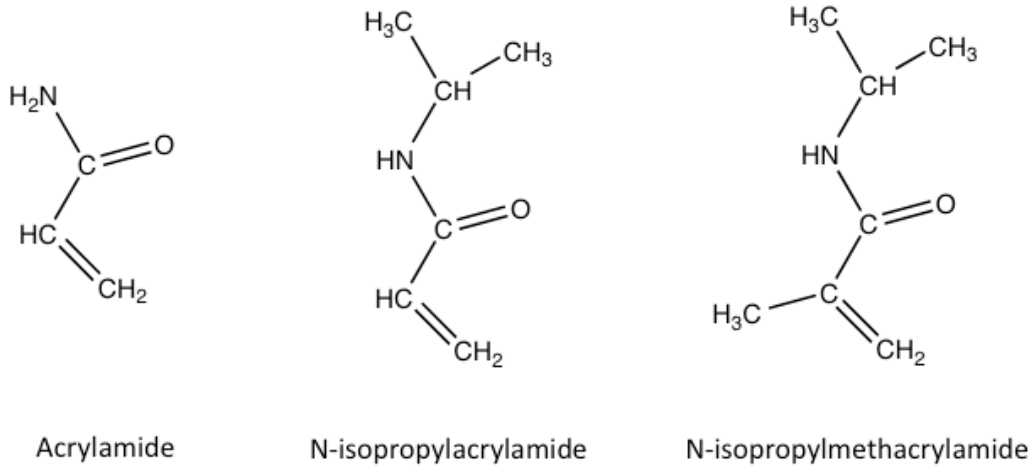

Figure 2.7. Chemical structures of various acrylamides.

2.3.1.1 Synthesis of acrylamide-based polymers

Radical chain polymerization is commonly used to synthesize acrylamide-based polymers. This technique is characterized by being initiated by a reactive species *R** produced from an initiator *I,* as shown in Equation 2.1.

$$I \rightarrow R\ *$$ **Equation 2.1**

The reactive species, commonly a free radical, adds to a monomer molecule by opening the π-bond to form a new radical. New monomer molecules are successively added to propagate the reactive center, as seen in Equation 2.2.

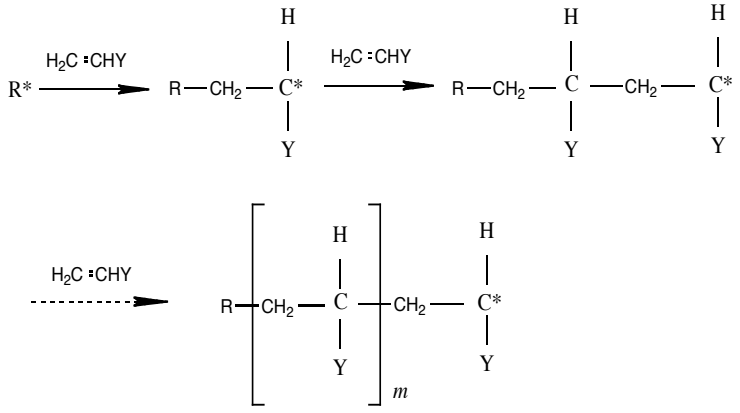

Equation 2.2

Chain growth is eventually terminated by a reaction with two reactive species.

Recent advances in radical polymerization focus on controlled radical polymerization (CRP) methods, which allow for higher control over molecular weights and end functionalities[60]. There are several different types of CRP techniques, including reversible addition-fragmentation chain transfer (RAFT), surfactant-free emulsion polymerization (SFEP), and surface-initiated atom transfer radical polymerization (SI-ATRP). These techniques are summarized in Table 2.2 below.

Table 2.2. Radical Chain Polymerization Techniques[61–63].

Surfactant-Free Emulsion Polymerization (SFEP) –polymerization initiator soluble in aqueous phase, polymer forms in oil phase –polymerization occurs at oil-water interface	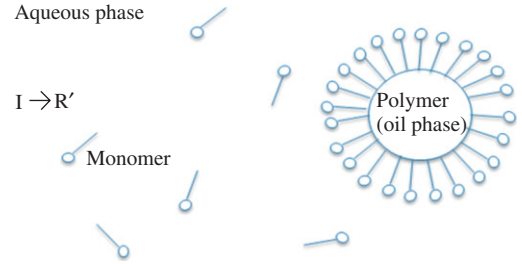
Reverse-Addition Fragmentation Polymerization (RAFT) –requires initiator in presence of chain-transfer agent –living polymerization technique	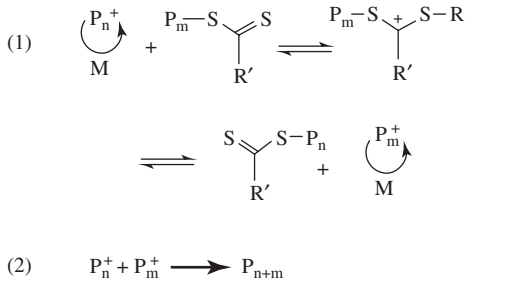
Surface Initiated-Atom Transfer Radical Polymerization (SI-ATRP) –requires a transition metal catalyst, nitrogen-based ligand, and alkyl-halide	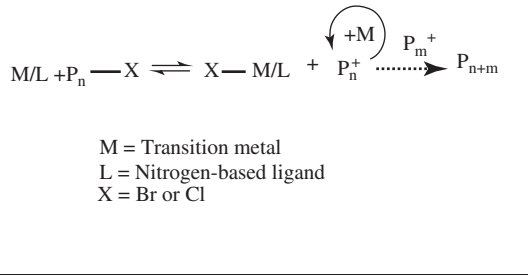

2.3.2 Elastin-like polypeptides

Elastin-like polypeptides (ELPs) are synthetic peptides derived from the sequence of the hydrophobic domain of tropoelastin[64]. ELPs generally consist of oligiomeric repeats of the pentapeptide VPGXG (where X is any amino acid except proline)[64]. By using recombinant methods to create these polymers, a monodisperse product with little batch-to-batch variability can be achieved, which is highly advantageous over chemically synthesized polymer materials[51–53]. By altering amino acid sequence or number of repeats, ELP LCSTs (also commonly called transition temperatures, or T_t) are highly tunable and can be brought to above physiologic temperatures[52,53]. ELPs are synthesized by creating the genetic

sequence that encodes these repetitive polypeptides, inducing expression of that sequence in *E. coli*, and then purifying the peptide product. This is commonly done through a process known as recursive directional ligation (RDL), which allows the synthesis of large, repetitive genes[52].

2.3.3 Thermally-responsive polymers in cancer medicine

Many of the first comprehensive studies of a thermally responsive polymer being used in a cancer medicine studies come from the Chilkoti group[53,65–71]. The first of such, published in 2001, showed that ELPs conjugated to drugs could be thermally targeted to solid tumors[65]. ELPs were designed to have a T_t of ~41^{o}C, with the hypothesis that these particles would remain soluble in solutions below their T_t (such as at physiologic temperature), but then become insoluble and aggregate at solution temperatures above 41^{o}C. These particles could then be injected and would circulate throughout the body at 37^{o}C, however, if localized hyperthermia treatments were used to heat a solid tumor, these particles would become insoluble and aggregate in the tumor. For this study, ELP-rhodamine conjugates were injected in nude mice with human SKOV-3 ovarian carcinoma tumors with four study groups: (1) ELP1, designed to have a T_t at 41^{o}C, injected with tumor heating, (2) ELP1 injected without tumor heating, and (3) ELP2, designed with a high T_t to remain soluble at temperatures above 42^{o}C, with tumor heating, and (4) ELP2 without tumor heating. The results, illustrated in Figure 2.8, show a ~2 fold increase in tumor localization for group 1 compared to group 2, and significantly more accumulation for group 1 compared to all other groups ($p<0.001$)[65]. Additional studies by the Chilkoti group[68] yielded similar results and demonstrated that thermal cycling of the tumor between 37^{o}C and 41^{o}C further enhances ELP accumulation[69].

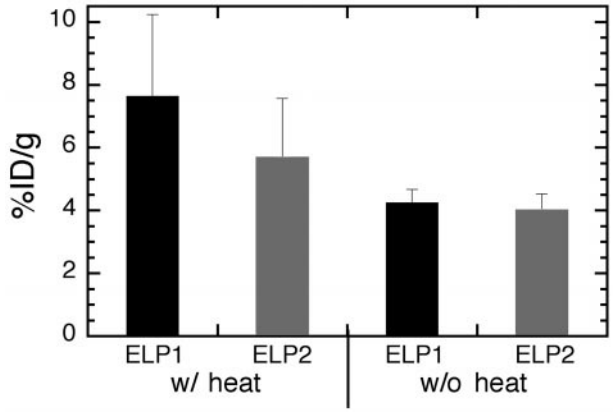

Figure 2.8. Tumor localization of ELPs. Expressed as percentage of the injected dose per gram of tissue. Tumor localization is significantly greater for the thermally responsive carrier (ELP1) when the tumor was heated to 42 ^{o}C compared to the other 3 groups ($p<0.001$). From Dreher *et al.* 2007[69].

A similar study compared the ability to target both thermally responsive ELPs and thermally responsive poly(NIPAAm-co-AAm) to tumors[53]. In this study, both the ELP and poly(NIPAAm-co-AAm) used were tuned to have an LCST at 40^{o}C. This was accomplished by substituting Ala and Gly residues for the more hydrophobic Val at the fourth position of the ELP pentipeptide, and by using an 84:16 ratio of NIPAAm:AAm in the poly(NIPAAm-co-AAm). In addition, a control ELP and polymer were made to have an LCST above 42^{o}C, and therefore remained soluble even in the heated tumor. Results, shown in Figure 2.9, indicate that heating did increase accumulation of both thermally responsive carriers in the tumor compared to controls. However, the ELP displayed enhanced accumulation in tumors over the polymer. The authors speculate that this may be because the LCST of poly(NIPAAm) and its copolymers can only be tailored to a limited extent by altering incorporation of co-monomers, chain length, sequence, and stereochemistry, whereas ELPs genetic control allows for more precise tuning of chemical properties such as transition temperature[53].

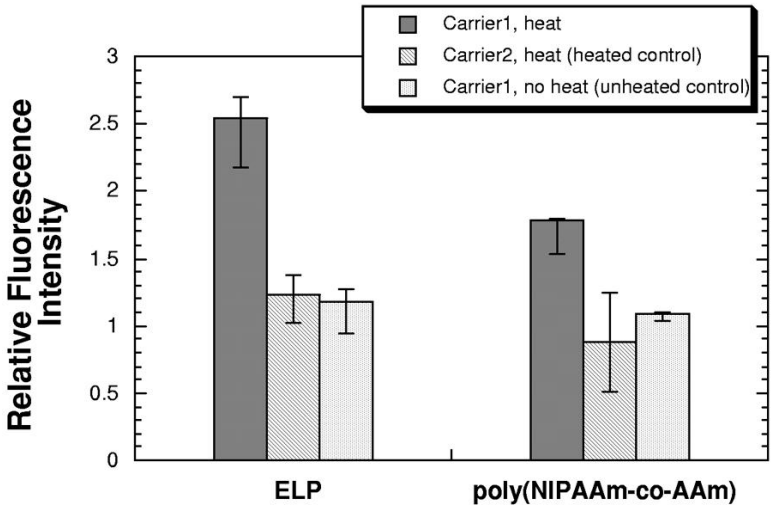

Figure 2.9. Tumor accumulation of ELPs and polymer carriers. Total fluorescence intensity for ELP and polymer carriers at 44 and 26 minutes post-injection, respectively. Carrier 1 was the thermally responsive carrier (LCST ≈ 40 ^{o}C) and Carrier 2 was the control carrier (LCST > 42 ^{o}C). From Meyer *et al.* 2001[53].

In a study by Dreher *et al.*, the chemotherapeutic doxorubicin (dox) was conjugated to ELPs through an acid-labile hydrazine bond, aimed to release the drug within the acidic environment of lysosomes[66]. Further optimization of ELP-dox conjugates analyzed the effects of: (1) the site of dox attachment to the ELP, (2) different acid-labile bonds for optimal release, and (3) design of a linker in which the acid labile bond is embedded[67]. It was found that the attachment to the C-terminal cysteine residue was optimal. Linker structure seemed to have little effect on the T_t of the ELP, but the shortest linker tested displayed the highest release of dox at ~80% released at 72 hours at pH 4[67].

A study by MacKay *et al.* analyzed the *in vivo* efficacy of an ELP-like drug carrier loaded with doxorubicin[70]. These carriers, called chimeric polypeptides (CPs) consisted of two segments: a biodegradable ELP segment and a short segment for the attachment of dox.

These particles self-assemble into sub-100 nm nanoparticles upon drug attachment, as demonstrated in Figure 2.10[70].

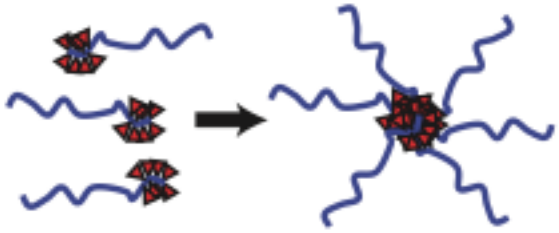

Figure 2.10. Self-assembly of chimeric polypeptides. The hydrophobic drug triggers self assembly into a particle with a drug rich core (red triangles) surrounded by hydrophilic polypeptide corona (blue chains). From MacKay *et al.* 2009[70].

These particles were injected into a mice BALB/c subcutaneous mouse tumor model via a tail vein injection (5 mg doxorubicin equivalent/kg). Tissue biodistribution of the particles was analyzed at both 2 and 24 hours post-injection. After 24 hours post administration, tumor tissue had a 3.5-fold increase in dox concentration for the CP-dox group compared to the free dox group. In addition, the CP-dox group showed decreased dox concentration in several tissue sites known to be adversely affected by dox including the muscle, lung, and heart[70]. A survival analysis of mice receiving either CP-dox or free dox found that CP-dox treatment cured 8 of 9 mice for up to 66 days post tumor implantation, while the median survival for a PBS injection (control) was 21 days and for free dox administration was 27 days[70]. It is interesting to note that this study did not utilize the thermal properties of the CP particles, as the tumor was not heated as had been done in previous studies. Further studies from the Chilkoti group have looked at ELP-radionuclide conjugate effects of tumor progression[71]. Additionally, other groups have looked at ELPs as delivery vehicles for short peptides to disrupt transcriptional functions[72].

2.4 THERMALLY RESPONSIVE POLYMER-NANOPARTICLE COMPOSITES

Thermally responsive polymer-metal nanoparticle composites couple the ability of metal nanoparticles to convert external stimuli to heat with polymers that display sharp property changes in response to temperature changes, allowing for external control over polymer properties. These systems have been investigated for a variety of biomedical applications, including drug delivery, microfluidic valve control, and cancer therapy. Three size scales of this system have been investigated: bulk systems (>1 mm), nano/micro scaled systems, and individual particle coatings. Previous studies of such systems relating to biomedical applications are discussed in this section.

2.4.1 Bulk Systems

Several systems incorporating bulk hydrogels (diameter >1 mm) with encapsulated nanoparticles have been investigated for applications including drug delivery[29,30,35,73], microfluidic[33,34,74] and microlens[75] control. Additionally, the effects of these encapsulated nanoparticles on polymer bulk properties have been studied[76,77].

Drug delivery applications using both near-infrared absorbing nanoparticles and iron oxide nanoparticles are of interest. By combining thermally responsive polymers with encapsulated nanoparticles, drug release can be triggered by an external stimulus, A schematic of this process is shown in Figure 2.11.

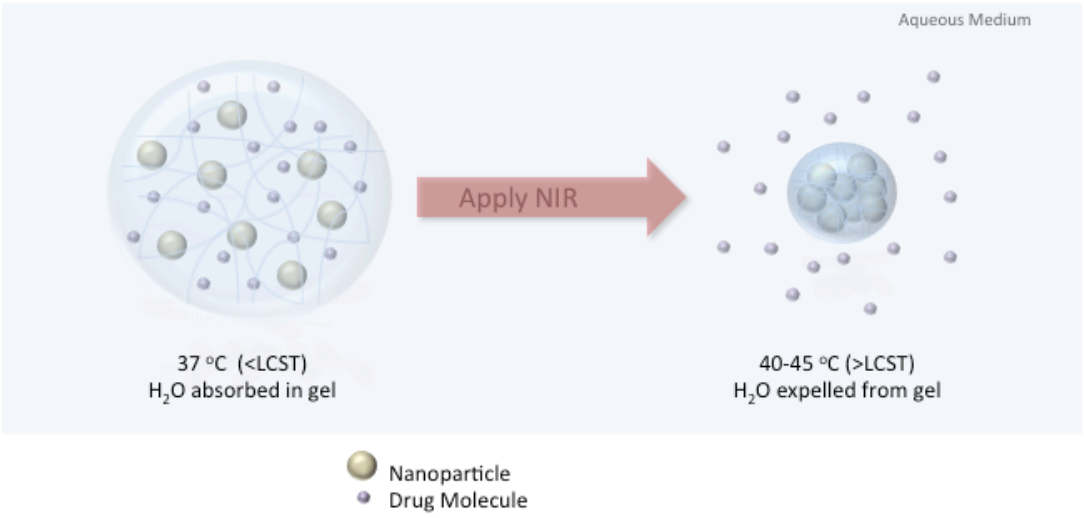

Figure 2.11. Schematic of drug delivery from bulk hydrogels.

Photothermally modulated drug delivery was first shown by Sershen *et al.* using a combination of N-isopropylacrylamide-co-acrylamide (NIPAAm-co-AAm) and gold-gold sulfide nanoparticles[29]. This study used hydrogels with a 95:5 molar ration of NIPAAm:AAm to achieve an LCST slightly above physiologic temperature. Upon NIR irradiation of these composites, the temperature of the hydrogel exceeds the LCST causing a burst release of any soluble molecules contained in the hydrogel matrix. Enhanced release of molecules such as methylene blue, ovalbumin, and bovine serum albumin was found to follow near infrared irradiation of the nanoparticle-composite hydrogels[29]. Further investigation of this system showed that it could be applied to photothermal delivery of insulin[30].

A system using the same NIPAAm:AAm hydrogel formation with gold-silica nanoshells also successfully demonstrated photothermal drug delivery[35]. Studies showed that

the collapse of hydrogel-nanoshell composites was controlled by both laser fluence and SiO_2 nanoshell concentration[35]. Photothermal release studies of methylene blue, insulin and lysozyme showed a pulsatile drug release that was dependent on the molecular weight of the molecule[35].

Magnetic iron oxide particles embedded in a NIPAAm- based matrix[73,78–80] have also been investigated for use as a drug delivery system, Bulk hydrogels were created using tetra(ethylene glycol) dimethacrylate (TEGDMA)[73,80] or poly(ethylene glycol) 400 dimethacrylate (PEG400DMA)[79] as a crosslinking agent. The incorporation of varying concentrations of iron oxide particles (20-30nm diameter) showed no effect on swelling characteristics of the hydrogels[78]. These hydrogel discs were found to increase in temperature and then collapse following exposure to an alternating magnetic field (AMF)[73,79]. A burst release of absorbed methylene blue or vitamin B12 followed pulse application of AMF, with minimal diffusion of the particles out of the matrix without AMF[73]. This study discussed that such a composite could potentially be used as a implanted, remotely controlled drug delivery device[73].

2.4.2 Nano/Micro Scale Composites and Micelles

While the majority of applications in this field focus on either bulk (>1mm) hydrogels or nanoscale coatings, a few groups have looked at micro-sized applications and micelles. Investigations have focused mostly on electrical and sensor properties of these materials[81–83] as well as their potential for drug delivery[84,85].

A study by Kim *et al.* proposed combining hybrid AuNP/iron oxide NPs with a poly[N-isopropylacrylamide-co-acrylamide]-block-poly[ε-caprolactone] for combined

hyperthermia and chemotherapy delivery with optical imaging[84]. This study used an 86:14 NIPAAm:AAm ratio to achieve an LCST of 42-45^{o}C. Initial results showed that the hydrodynamic diameter of these micelles decreased from 104 nm to 71 nm when temperature was increased from 25^{o}C to 45^{o}C. Further optical and magnetic studies and characterization of this system are ongoing[84].

Hoare *et al.* developed a membrane-based drug delivery system consisting of an ethyl cellulose-iron oxide particle nanocomposite membrane with embedded PNIPAAm-based hydrogels, as shown in the schematic in Figure 2.12[85]. By applying an oscillating magnetic field to this device, the heat increase caused the nanogel to deswell, allowing a "strong flux" of drugs out of the reservoir. This device was synthesized by coevaporation caus entrapment of PNIPPAm nanogels and iron oxide nanoparticles in the cellulose membrane. The PNIPAAm gel was engineered to have an LCST above physiologic temperature by incorporating NIPMAAm as well as AAm. Analysis with sodium fluorscein showed a ~20 fold increase in flux when the device was turned "on" by exposure to an oscillating magnetic field, as well as consistent drug flux over four on-off cycles. The authors noted that the rapid swelling kinetics due to the size and engineered phase-transition behavior of the nanogels as well as the optimized size and surface chemistry of the iron oxide nanoparticles allowed for rapid, repeatable, and tunable drug release under physiological conditions[85].

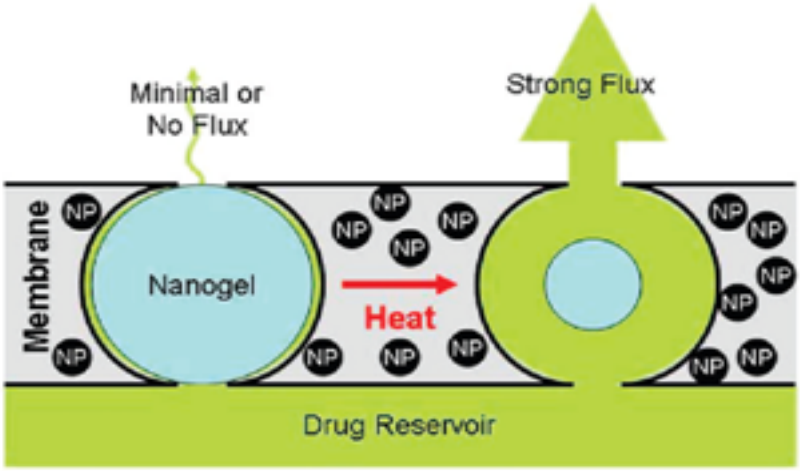

Figure 2.12. Schematic of drug delivery from magnetically triggered nanogel composite membranes. From Hoare *et al.* 2009[85].

2.4.2.1 Thermally Responsive Liposomes

Heat sensitive liposomes have been investigated for drug delivery applications, with some formulations reaching clinical trials[86]. Recent work by Qin *et al.* aimed to combine a heat sensitive liposome with gold nanoparticles attached to the surface[87]. The characteristics of this system are described in Figure 2.13 below.

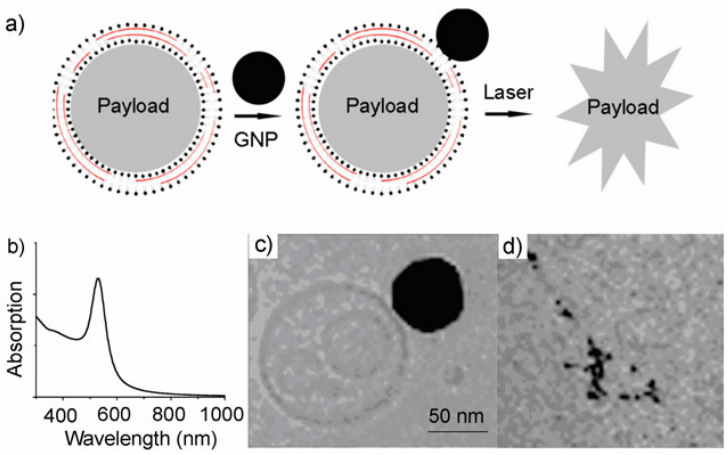

Figure 2.13. Properties of thermally responsive lipsome-gold nanoparticle system. (a) Schematic of drug release process. (b) UV-vis absorption spectrum of the gold nanoparticles used. (c) Cryo-TEM image of a liposome tethered to a gold nanoparticle (d) Cryo-TEM image of a liposome-nanoparticle complex after irradiation with a 532 nm laser. From Qin *et al.* 2011[87].

This system was tested with doxorubicin and was found to retain the encapsulated drug at 40^{o}C for 3 days and instantaneously release over 70% of the encapsulated drug upon exposure to a 532 nm laser. Further research is being done to tether hollow gold nanoshells, which have a surface plasmon peak in the near infrared range, instead of solid gold nanoparticles, to allow the system to be used in clinical applications[87]. Other groups have looked at remote control release from thermosensitive liposomes by injections of both liposomes and gold nanorods[88].

2.4.3 Polymer Coated Nanoparticles

As of late, much focus has been placed on ways to apply a thermally-responsive hydrogel coating on individual nanoparticles. This would allow particles to retain their size while gaining the drug delivery potential of PNIPAAm based systems discussed previously. Several synthesis methods have been investigated for this application including reversible

addition-fragmentation chain transfer (RAFT)[89–92], surfactant-free emulsion polymerization (SFEP)[36,93,94], surface initiated-atom transfer radical polymerization (SI-ATRP)[95–97], and other methods[98,99].

2.4.3.1 SFEP Methods

The work of Kim *et al.* investigates SFEP of poly(NIPAAm-co-AAc) onto AuNP and silica-Au nanoshells for drug delivery applications[36,93,94]. This synthesis method used a 94:6 wt% ratio of NIPAAm:AAc and N,N-methylenebisacrylamide (BIS) as a crosslinking agent. This process was carried out on 60 nm AuNP[93] and silica-Au nanoshells[36]. In addition, studies using a SFEP poly(NIPAAm-co-AAc) as a template for the growth of large (60-150nm) AuNP have also been investigated[94]. In the study utilizing gold-silica nanoshells, FE-SEM images showed uniform particle sizes as well as contrast effects showing particle cores with a complete hydrogel coating[36]. Energy-dispersive x-ray spectroscopy (EDX) analysis showed large peaks indicating gold atoms as well as no peaks for the hydrogel polymer, as predicted given the low atomic numbers of the hydrogel elements. Higher resolution TEM images show the complete hydrogel shell growth around the particle, as well as differences in hydrogel thickness that could be obtained by minor variations in the monomer and initiator amounts or reaction time. However, one drawback of this polymerization method is the encapsulation of multiple particles into one hydrogel matrix. UV-Vis spectroscopy showed minimal changes in the absorption profile of the bare Silica-Au nanoshells and hydrogel coated nanoshells. DLS studies showed that the hydrodynamic radius of the hydrogel particles decreased with increasing temperature, an indication of collapse of the hydrogel. The results of this study are summarized in Figure 2.14[36].

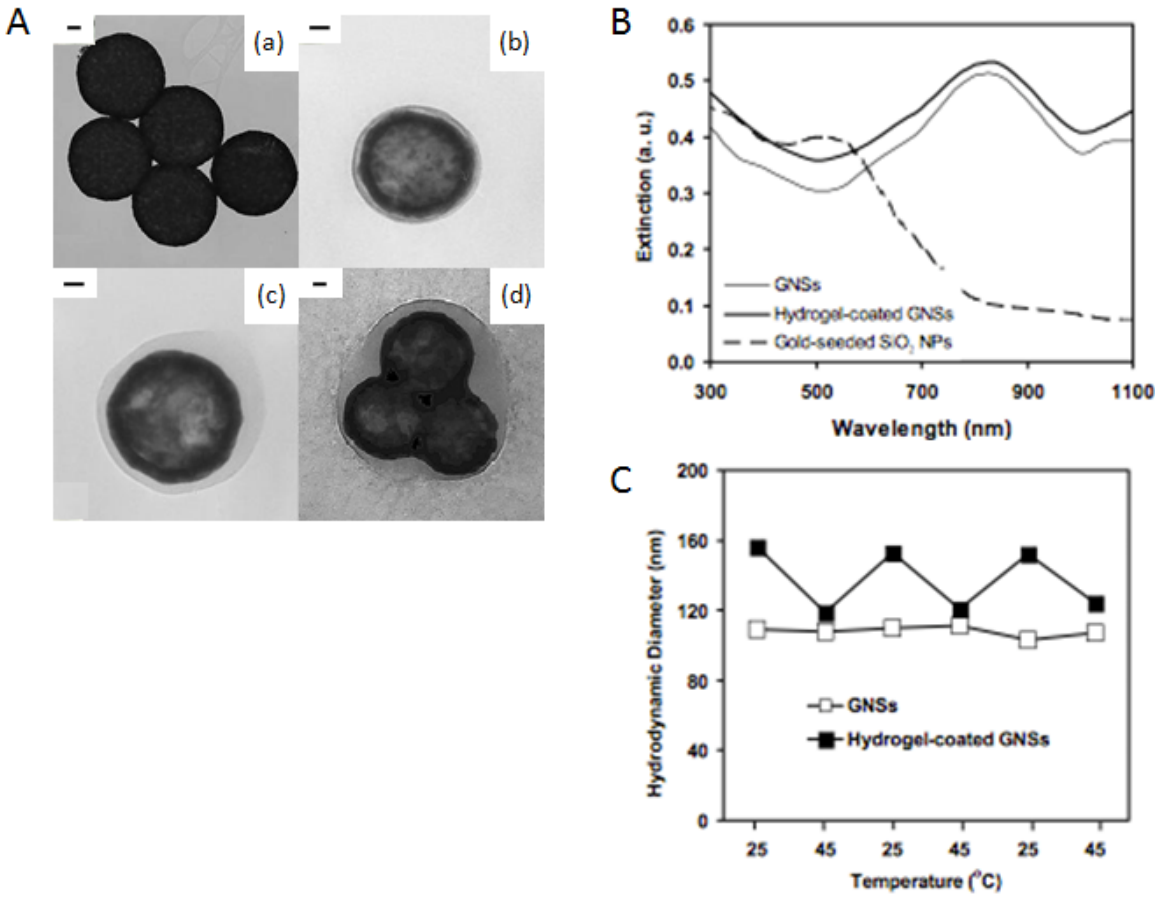

Figure 2.14. Hydrogel coating by surfactant-free emulsion polymerization (SFEP). [A] TEM images of (a) bare nanoshells (diameter~120 nm); (b) thin hydrogel-coated nanoshells (diamter~160 nm); (c) thick hydrogel-coated nanoshells; and (d) multiple encapsulated nanoshells. [B] UV-Vis spectra of gold-seeded silica cores, bare nanoshells, and hydrogel coated nanoshells. [C] Hydrodynamic diameters of bare nanoshells and hydrogel-coated nanoshells as a function of temperature. Adapted from Kim *et al.* 2008[36].

2.4.3.2 SI-ATRP Methods

Synthesis of a hydrogel coating using SI-ATRP has also been investigated due to its tight control over the thickness of gel produced, providing for monodisperse particles. Wei *et al.* used this method to create a PNIPAAm coating on NIR absorbing AuNRs[96]. This study used AuNRs with an aspect ratio of 4.4±0.4 and a peak longitudinal plasmon resonance of 843 nm. A disulfide initiator was immobilized onto the AuNR surface followed by *in situ*

polymerization of PNIPAAm. TEM characterization of the particles showed a core/shell structure was formed, and it was noted that the thickness of the coating could be tuned by the polarity of the solvent, with more polar solvents yielding thicker coatings. DLS showed an increase in hydrodynamic diameter at temperatures from 32-37^{o}C, indicating the hydrogel coatings had collapsed and become more hydrophobic, causing the particles to precipitate out of solution and aggregate. In addition, a drug loading experiment with norvancomycin, an antibiotic, showed increased release when the particles were irradiated with an 808 nm laser[96].

This method has also been employed using iron oxide nanoparticles. Frimpong *et al.* demonstrated growth of a PNIPAAm hydrogel with poly(ethylene glycol) 400 dimethacrylate (PEG400DMA) crosslinks using SI-ATRP on iron oxide particles of 6-10 nm diameters[95]. First, the particles were coated with either oleic acid or citric acid followed by a ligand exchange reaction with bromine alkyl halides and a bromo-saline to act as initiators of the ATRP reaction of poly(NIPAAm-PEG400DMA). High resolution TEM analysis showed an ordered crystalline core next to an amorphous polymer shell less than 5 nm thick. DLS analysis showed a larger hydrodynamic diameter of these particles at temperatures from 20-30^{o}C with smaller hydrodynamic diameters observed at temperatures above the hydrogel LCST[95].

2.4.3.3 Elastin-like polypeptide coatings

Huang *et al.* developed an optically responsive ELP-gold nanorod system[100]. A novel 22 kDa cysteine containing ELP was conjugated to NIR absorbing gold nanorods by gold-thiol bonds[103]. The transition temperature (T_t) of the ELP was determined to be 33.4^{o}C; above this temperature the particles aggregated together resulting in an increase in optical

density. NIR irradiation of these particles resulted in an optical response due to a conformational change in the ELP^{100}.

2.5 CONCLUSION

In the current literature, there is no report of an optically triggered thermally responsive polymer-nanoparticle drug delivery system that has been successfully tested *in vivo*. This thesis builds on the successful results from previous studies to create such a platform. This delivery platform was synthesized using two material components: a thermally responsive poly(NIPAAm-co-AAm) hydrogel and embedded gold-silica nanoshells. The controlled delivery system being proposed in this thesis aims to provide burst delivery of a cancer therapeutic only at the site of malignant tissue.

To begin, Chapter 3 of this thesis describes the synthesis and characterization of bulk poly(NIPAAm-co-AAm)-gold nanoshell composites. In Chapter 4, these composites are loaded with cancer therapeutics, and release is demonstrated to follow NIR light exposure. Chapter 5 describes methods being used to synthesize this platform as nanoscale-sized particles. Finally, Chapter 6 summarizes these results and discusses future optimization of this platform.

3 SYNTHESIS OF BULK HYDROGEL-NANOSHELL COMPOSITES

3.1 INTRODUCTION

This chapter presents the methods used throughout this thesis to synthesize and characterize gold-silica nanoshells, poly(NIPAAm-co-AAm) hydrogels, and hydrogel-nanoshells composites. This material was designed such that it would be swollen in physiologic state, but would collapse in response to NIR exposure.

3.2 GOLD-SILICA NANOSHELL SYNTHESIS

To synthesize gold-silica nanoshells, silica cores are created using the Stöber method and then surface functionalized with amine groups using silane reagents. Small gold colloid particles (~2 nm) were then absorbed onto the aminated surface to form gold nucleation sites[19]. A final reduction step in chloroauric acid, potassium carbonate, and formaldehyde produced a gold shell between 5-30 nm thick[18]. This synthesis process is summarized in Figure 3.1, accompanied by a TEM micrograph depicting shell growth[31].

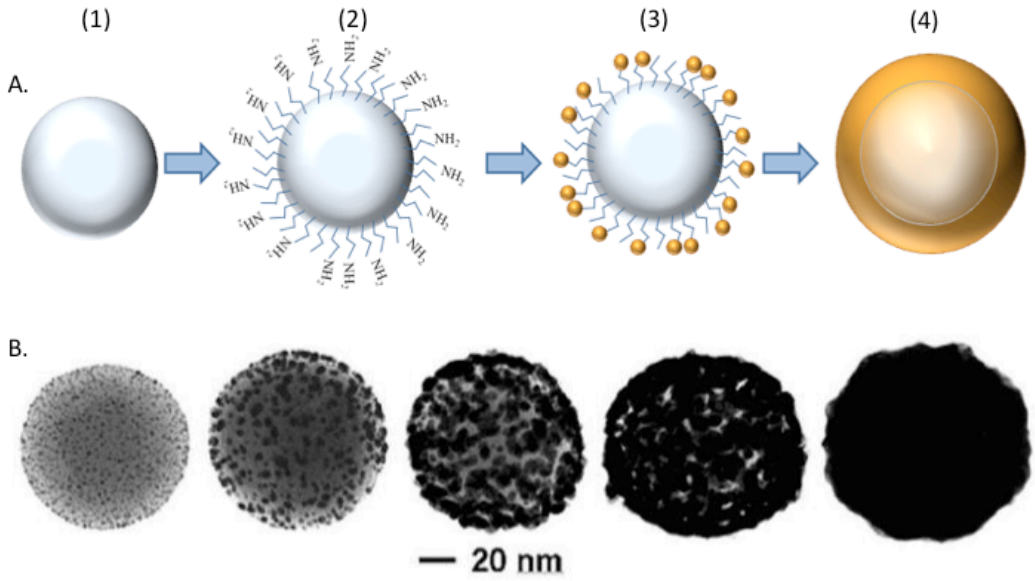

Figure 3.1. Gold-silica nanoshell synthesis. [A] The four steps of gold-silica nanoshell synthesis: (1) formation of silica core, (2) amine functionalization, (3) absorption of gold colloid and (4) shell growth. [B] TEM image depicting shell growth on a silica core from absorbed gold colloid. Adapted from Oldenburg *et al.* 1998[31].

For the first step of silica core formation via the Stöber method[101], tetraethyl orthosilicate (TEOS) was reduced in ethanol (EtOH) in the presence of ammonium hydroxide (NH_4OH). To achieve core diameters of approximately 120 nm, 0.5 g of NH_4OH (Aldrich, 28%) was added to 32.06 g 200 proof EtOH. With rapid stirring, 1.69 g of TEOS (Aldrich, 99.999%) was added. The reaction mixture was rocked overnight at room temperature. The following day the cores were washed by three rounds of centrifugation (2500g, 30 min) and suspended in EtOH. Scanning electron microscopy (SEM, FEI Quanta 400 FEG) was used to determine core diameters and polydispersity. Cores with a diameter of ~120 nm and polydispersity of <10% were used in subsequent steps. Silica cores were then functionalized with amine groups via a reaction with aminopropyltriethoxysilane (APTES). For every 1 ml of cores at 4 wt%, 5 µl of APTES (Gelest) was added under rapid stirring and allowed to

react overnight at room temperature. The following day, the reaction solution was boiled for 2 h to ensure surface exposure of amine groups. The solution was then centrifuged for 3 rounds (2500xg, 30 min) and resuspended in EtOH.

Colloidal gold particles with a 2-4 nm diameter were prepared by a reduction of chloroauric acid ($HAuCl_4$) as previously described in the literature[102]. A solution of tetrakis(hydroxymethyl)phophonium chloride (THPC, TCI America, 80%) in water was created by mixing 400 µl of THPC with 33 ml millipore H_2O. Next, 4 ml of this THPC solution was added to 1.2 ml of 1 N sodium hydroxide (NaOH, Aldrich) and 180 ml of millipore H_2O. This solution was rapidly stirred for at least 5 min, and then 6.75 ml of 1% $HAuCl_4$ (Alfa Aesar, 99.999%) was added. The solution was stirred until the solution color stabilized (<1 min) and the product was stored at 4 ^oC. This colloid solution was aged for at least 2 weeks before being used in subsequent steps.

Aminated silica cores were then mixed with this gold colloid suspension to create "seed" particles with the colloid being absorbed onto the silica core via electrostatic interaction between the positively charged amine group and negatively charged colloid. For this reaction, 30 ml of colloid suspension was mixed with 180 µl functionalized cores and 1 ml 1 M NaCl. The reaction mixture was rocked for at least 48 h at room temperature and washed by two rounds of centrifugation (1500xg, 30 min) and resuspended in H_2O.

Nanoshell synthesis was completed by a shell growth step. A gold plating solution was made by combining 200 mg of potassium carbonate (K_2CO_3), 12 ml of 1% $HAuCl_4$, and 800 ml H_2O. Various seed particle volumes (200-500 µl) were added to 1 ml of the plating solution. 10 µl of formaldehyde (HCHO, 37%) was added to the solution with rapid mixing.

This causes a reduction reaction in which the absorbed colloids of the seed particles serve as nucleation sites for shell growth by additional reduced gold ions. Formulations that produced particles with an extinction profile peak near 800 nm were linearly scaled up. After synthesis, nanoshells were washed by one round of centrifugation (1500xg, 10 min) and resuspended in 1.81 mM K_2CO_3 for storage. Before use in subsequent applications, stored nanoshells were washed via one centrifugation round (1500xg, 10 min) and resuspended in H_2O.

As synthesized, these particles were found to have a diameter of 153.65 (±8.96) nm. A TEM image of synthesized gold-silica nanoshells and their extinction spectra is shown in Figure 3.2 below.

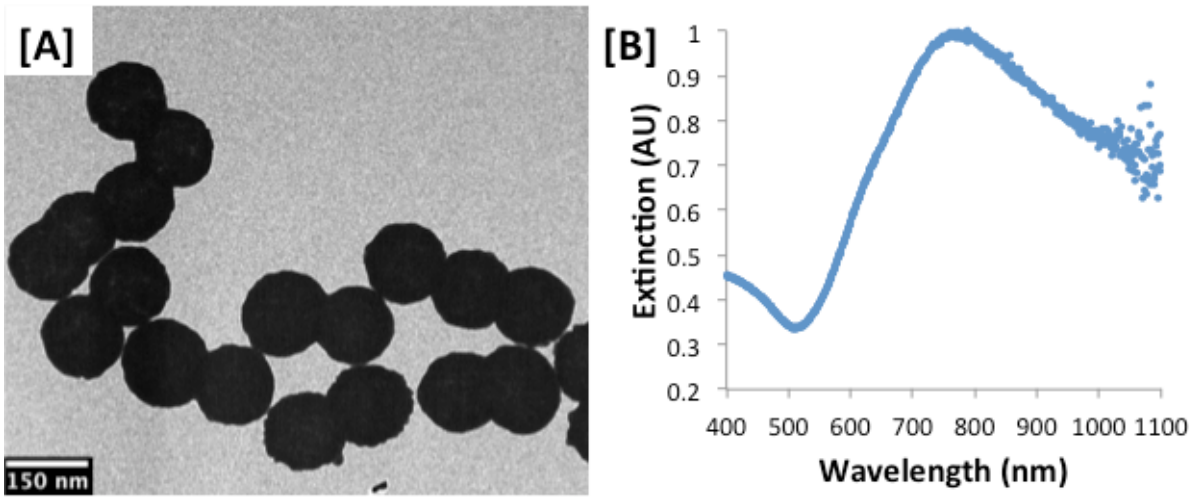

Figure 3.2. Gold-silica nanoshell characterization. [A] TEM image of synthesized gold-silica nanoshells. [B] Extinction spectra of synthesized gold-silica nanoshells. Particles were synthesized to have maximum light absorption in the NIR region.

3.3 Poly(NIPAAm-co-AAm) Hydrogel Synthesis

Poly(NIPAAm-co-AAm) hydrogels were synthesized using free radical polymerization. Prior to synthesis, NIPAAm (Aldrich, 97%) was dissolved in tetrahydrofuran (THF) and recrystallized in *n*-hexane. This step removes the small molecule inhibitor *p*-

methoxyphenol from the packaged NIPAAm. The recrystallization process was repeated at least 3 times and the final product was dried by lyophilization and stored at -20^{o}C. Stock solutions of NIPAAm (1.75 M), AAm (Sigma, ≥99%, 15 M), and *N,N'*-methylenebisacrylamide (MBAAm) (Sigma, ≥98%, 0.169 M) were made in water. A prepolymer solution of a 95:5 molar ratio of NIPAAm:AAm and a 1:750 molar ratio of monomer:crosslinker (MBAAm) was created from the stock solutions: 3.56 ml 1.75 M NIPAAm, 21.88 µl 15 M AAm, and 51.78 µl 0.169 M MBAAm and 116.34 µl H_2O were added to a three-neck round bottom flask (3.75 ml total). Argon (Ar) gas was bubbled through this solution for at least 15 min in order to remove dissolved O_2, which inhibits the polymerization process. With rapid stirring, 37.5 µl of 10% (w/v) ammonium persulfate (APS, Sigma-Aldrich, ≥98%) and 7.5 µl of *N*,*N*,*N*′,*N*′-tetramethylethylenediamine (TEMED, Sigma, ≥99%) were added to initiate the redox reaction for free radical polymerization. Composite hydrogels were synthesized in a similar fashion, with 8x10^{9} nanoshells/ml being added to the prepolymer solution prior to adding APS/TEMED. The polymerization solution was then quickly poured into a mold consisting of 2 glass slides separated by a 1.5 mm Teflon® spacer held together by metal clamps. The hydrogel was then cured at 30^{o}C for 2 h under vacuum. After curing, the hydrogel slab was soaked in 95% EtOH for at least 12 h followed by H_2O for at least 12 h to remove any organic solvents and unreacted monomers. Hydrogel disks of a 4 mm diameter were punched out with a cork borer. A schematic of this polymerization process is shown in Figure 3.3 below.

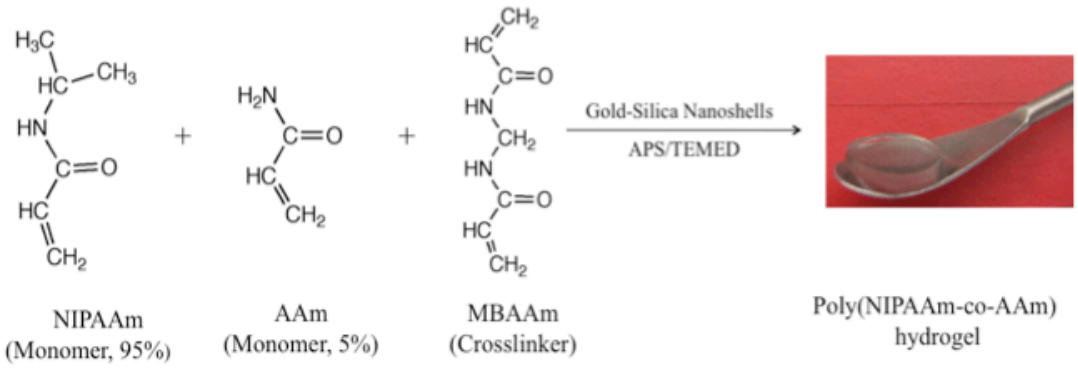

Figure 3.3. Poly(NIPAAm-co-AAm) hydrogel synthesis. A solution of a 95:5 molar ratio of the monomers NIPAAm:AAm and a 1:750 ratio of crosslinker MBAAm:monmers is polymerized by free radical polymerization initiated by APS and TEMED.

3.4 Thermal Analysis of Hydrogel-Nanoshell Composites

After synthesis, the swelling behavior of the poly(NIPAAm-co-AAm) gels was analyzed in response to temperature. The hydrogels were allowed to swell at room temperature (22°C) for at least 24 h before testing. To determine the LCST of the hydrogels, the gels were first weighed and placed in TRIS buffer (pH 7.4) and then incubated at various temperatures (29°C, 33°C, 37°C, 41°C, 45°C, and 50°C) for 10 min. After incubation, the gels were weighed again, and the deswelling of the gel was calculated using Equation 3.1 below.

$$\textit{Deswelling Ratio}\ (\%) = 100 * \frac{Weight_{Temp}}{Weight_{Temp=22^oC}} \qquad \textbf{Equation 3.1}$$

Results, illustrated in Figure 3.4, show that these gels tend to collapse from 39-45°C, a temperature range slightly above physiologic temperature.

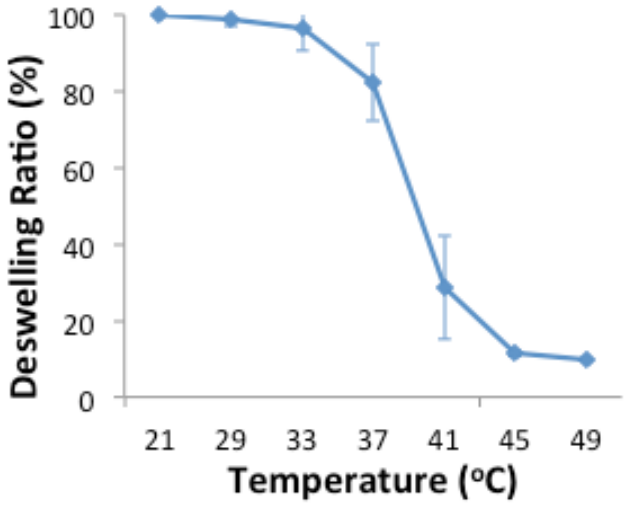

Figure 3.4. LCST of poly(NIPAAm-co-AAm) hydrogels. Deswelling of NIPAAm-co-AAm hydrogels as a function of temperature. These hydrogels collapse between 39-45°C. Deswelling ratio was calculated using Equation 3.1.

Next, the thermal behaviors of hydrogels with and without nanoshells were compared. These gels were either incubated in 2 ml TRIS buffer (pH 7.4) in a 50°C water bath or exposed to an NIR laser (Coherent Diode, 808 nm, 8 W/cm^2, 30 min). Gels were weighed every 10 min for 30 min and the deswelling of the gel was calculated using Equation 3.2.

$$\textit{Deswelling Ratio}\ (\%) = 100 * \frac{Weight_t}{Weight_{t=0}} \qquad \textbf{Equation 3.2}$$

Results are shown in Figure 3.5. Both gels with and without nanoshells displayed similar behavior when incubated at 50°C, indicating that the presence of nanoshells did not inhibit hydrogel collapse. When exposed to the NIR laser, gels with nanoshells deswelled similarly to the gels incubated at 50°C, while gels without nanoshells exhibited minimal deswelling in response to the laser. This demonstrated that both the presence of nanoshells

and exposure to an NIR laser were required to cause gel deswelling when heating with NIR light.

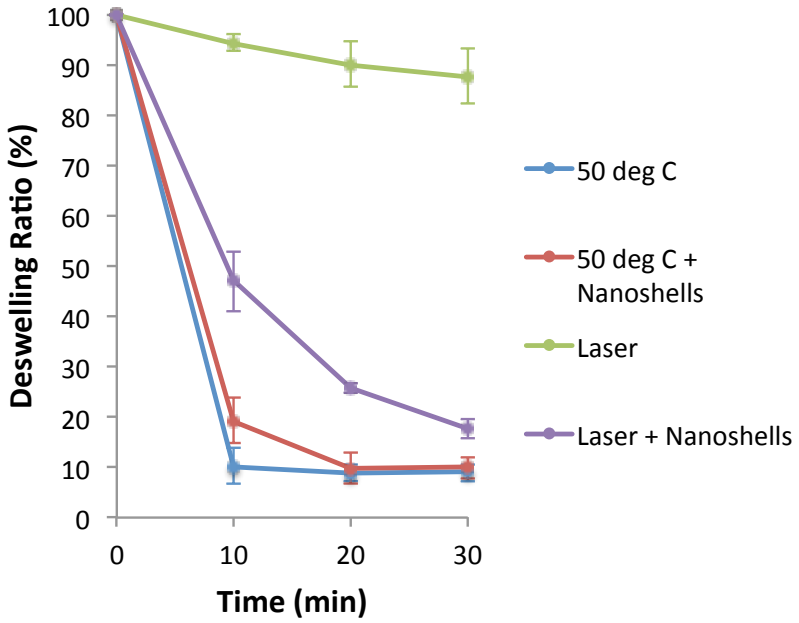

Figure 3.5. Deswelling in response to temperature changes and irradiation. Deswelling of NIPAAm-co-AAm hydrogels with and without nanoshells by either incubation in a 50°C water bath or exposure to an NIR laser. Deswelling ratio calculated using Equation 3.2.

3.5 Conclusions

In this chapter, a poly(NIPAAm-co-AAm)-gold nanoshell composite material was synthesized. This material has an LCST of around 39-45°C, meaning it will be swollen at physiologic temperature. Expulsion of absorbed water and collapse of the material was found to follow both incubation at 50°C and exposure to a NIR laser. With these results, we moved forward to use this optically induced phase transition to trigger drug release from the material, as described in Chapter 4.

4 THERAPEUTIC DELIVERY FROM HYDROGEL-NANOSHELL COMPOSITES

After analysis of the thermal deswelling of the bulk poly(NIPAAm-co-AAm) hydrogels, delivery studies of two different cancer therapeutics were performed: the chemotherapeutic doxorubicin (dox) and ssDNA as a model molecule for siRNA. A comparison of the two therapeutics is found in Table 4.1 below.

4.1 DESCRIPTION OF THERAPEUTICS

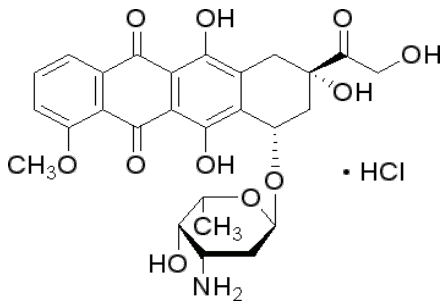

Figure 4.1. Chemical structure of doxorubicin.

Doxorubicin is a small molecule (580 Da) chemotherapeutic indicated in a wide variety of cancers including hematopoietic malignancies; carcinomas of the breast, lung, ovary, stomach, and thyroid; and sarcomas of bone and soft tissue[7]. The chemical structure of doxorubicin can be seen in Figure 4.1. Its optical properties allow for observation via both absorbance and fluorescence[103]. Doxorubicin, first known as an anthracycline antibiotic, was discovered to have anti-tumor effects in the 1960s[104]. The primary mechanism of action is intercalation with DNA during replication, causing inhibition of topoisomerase II binding and arrest of cell replication[105]. Side effects of doxorubicin include myelosuppression,

mucositis, and cardiac toxicity; furthermore, these side effects often cause patients to cease doxorubicin therapy, even if the drug is still effective against their malignancy[1].

The second therapeutic analyzed was single-stranded DNA (ssDNA), used as a model molecule for siRNA. Typical siRNAs are double-stranded with sticky ends and have a molecular weight of 13-15 kDa. Details regarding the mechanism of action of siRNAs can be found in Section 1.3.1. This study employed a 21 base pair oligonucleotide equivalent in sequence to the siRNA used to target the EphA2 protein. EphA2 is a receptor tyrosine kinase known to be upregulated in many cancers, Its functions include signaling involved in cell-cell contacts, cell migration, and angiogenesis[106]. Down regulation of EphA2 has been shown to reduce tumorigenecity in preclinical studies of several cancer types, including pancreatic and breast carcinomas[107].

Table 4.1. Comparison of Doxorubicin and siRNA.

	Doxorubicin	siRNA
Drug type	Chemical	Biologic
Size	580 Da	13-15 kDa
Chemical Properties	Hydrophobic	Hydrophillic
Intracellular Transport	Passive diffusion	Endosomal
Mechanism of Action	Inhibition of topoisomerase II	Prevents translation of complimentary mRNA sequences
Benefits for controlled delivery	Minimize off-site toxicity	Increase serum stability
Detection methods	Absorbance (485 nm) or fluorescence (585 nm)	Absorbance at 260 nm

4.2 THERAPEUTIC RELEASE FROM COMPOSITES

First, hydrogels with and without nanoshells were dried under vacuum for at least 48 h prior to drug loading. The dry weights of the gels were recorded. For the doxorubicin trials, the gels were then soaked in a 0.5 mg/ml (862 mM) solution of doxorubicin (Sigma) in TRIS buffer (pH 7.4) at 4^{o}C for at least 24 h. Absorbance readings of loaded gels were used to determine the loaded concentration of doxorubicin. For the dsDNA trials, the gels were soaked in a 25 mM solution of ssDNA (Invitrogen) in DNase free H_2O at 4^{o}C for at least 24 h. The concentration of ssDNA in the loaded gels was determined by measuring the ssDNA concentration of the soak solution before and after gel soaking.

Loaded gels were placed in TRIS buffer (doxorubicin gels) or DNAse free H_2O (ssDNA gels) and then either incubated at 50^{o}C for 30 min in a water bath or exposed to an NIR laser (Coherent Diode, 808 nm, 8 W/cm^2, 30 min). In addition, control gels with nanoshells were kept at room temperature (22^{o}C) for 30 min. Every 5 min, a buffer sample was analyzed for drug content. To determine doxorubicin concentration, absorbance at 485 nm was used to extrapolate a concentration value based on a standard curve (R^2 = 0.99968). DNA concentration was determined by absorbance at 260 nm using a Nanodrop® spectrophotometer.

Release of both doxorubicin and dsDNA from poly(NIPAAM-co-AAm) gels was then analyzed. Figure 4.2 shows release from gels in response to incubation at 50^{o}C, and Figure 4.2 shows release from gels in response to an NIR laser. Gels incubated at 50^{o}C with and without nanoshells showed similar release profiles, indicating that the presence of

nanoshells did not affect drug release. Approximately 77% of the loaded doxorubicin and 85% of the loaded ssDNA were released within 30 minutes.

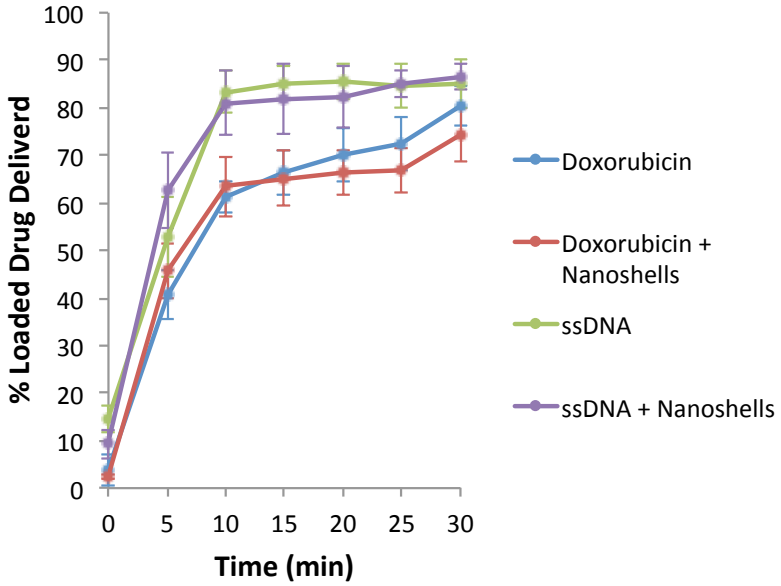

Figure 4.2. Drug release due to incubation. Drug release from poly (NIPAAm-co-AAm) hydrogels with and without nanoshells in response to incubation at 50°C.

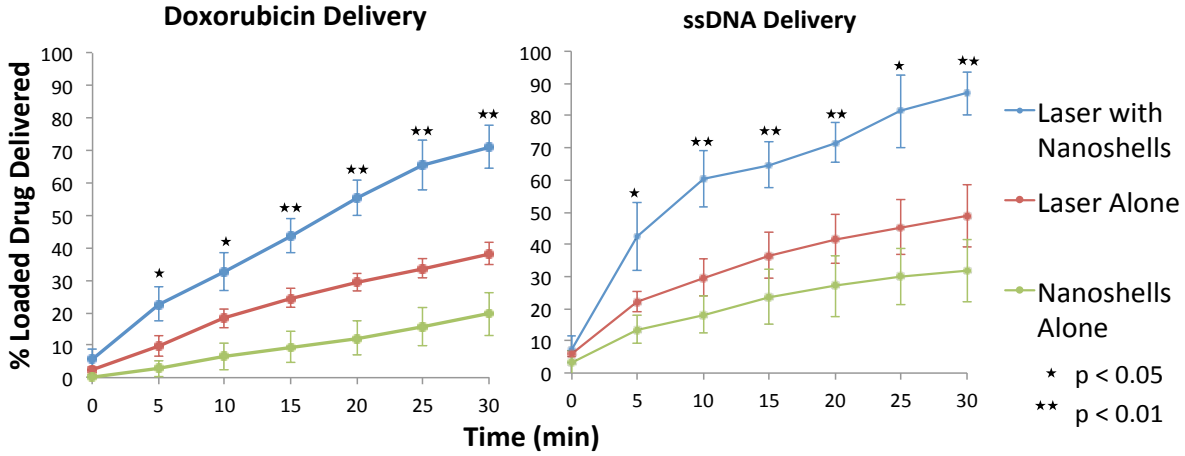

Figure 4.3. Drug release in response to NIR irradiation. Irradiated gels with nanoshells provide increased drug delivery over controls at all times t>0 ($p<0.05$).

Doxorubicin and ssDNA delivery after NIR irradiation indicated that nanoshell-composites provide increased drug release over controls for all times t>0, as analyzed by a two-sided t-test with a 95% confidence interval. Results from this study indicated that delivery of cancer therapeutics from a poly(NIPAAm-co-AAm) –nanoshell composites could be triggered by exposure to NIR light.

4.2.1 Delivery of double-stranded DNA (dsDNA)

In addition to initial validation of siRNA delivery using a ssDNA oligo, further tests were completed using double-stranded DNA (dsDNA) instead of ssDNA, as this is more similar to siRNA, which is also double stranded. Two properties of dsDNA are important to consider when using this delivery platform. First, ssDNA oligos are significantly more flexible than dsDNA oligos since they do not form a helix[108,109]. Second, dsDNA oligos are more thermally-sensitive, as the two strands are held together by supramolecular interactions such as hydrogen bonding, whereas the bonds between bases in ssDNA are predominantly covalent. For this study, a 21 base pair dsDNA oligo was loaded into gels, and release was measured in response to NIR irradiation. In addition, delivered DNA oligo integrity was assayed using poly(acrylamide) gel electrophoresis (PAGE).

Therapeutic loading into the gels was performed similarly to methods described in Section 3.2. Gels were soaked in a 17 mM solution of dsDNA (Integrated DNA Technologies, inc.) in duplex buffer (Integrated DNA Technologies, inc.) at 4^{o}C for at least 24 h. Loaded gels were placed in duplex buffer gels and then either exposed to an NIR laser (Coherent Diode, 808 nm, 8 W/cm^2, 30 min) or left at room temperature for 30 min. Every 5 min, a buffer sample was analyzed for drug content. DNA concentration was determined by

absorbance at 260 nm using a Nanodrop® spectrophotometer. Results are shown in Figures 4.4 and 4.5.

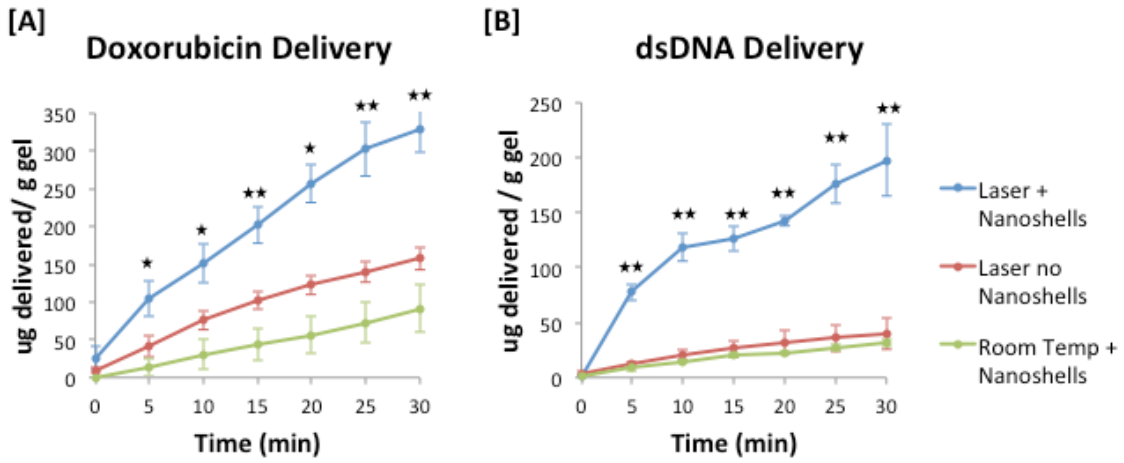

Figure 4.4. Delivery of [A] doxorubicin and [B] dsDNA in response to NIR irradiation. (*p<0.05, **p<0.01 as compared to laser no nanoshells).

Results from Figure 4.4 indicated that delivery of both chemical and biological cancer therapeutics, such as doxorubicin and dsDNA, can be triggered by exposure to NIR light. A closer look at ssDNA vs dsDNA delivery from these composites is shown in Figure 4.5.

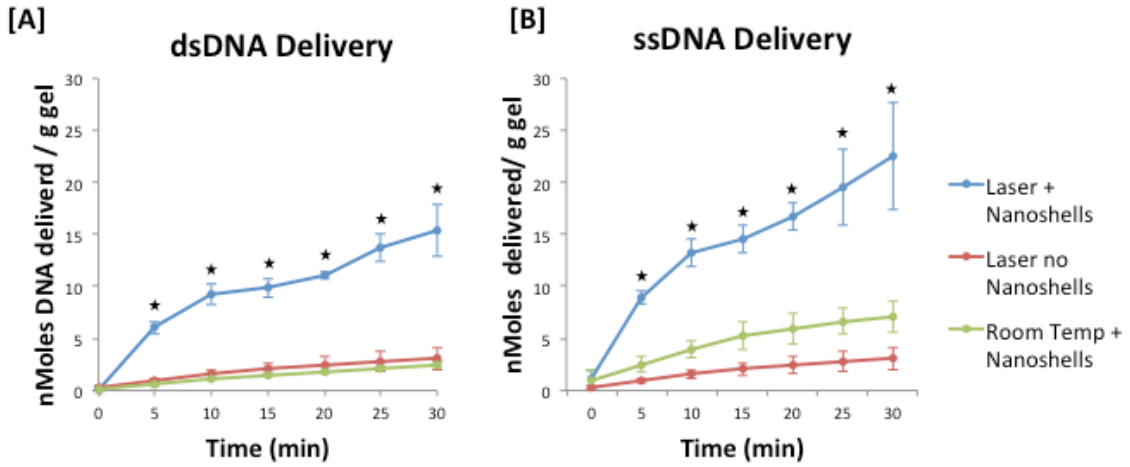

Figure 4.5. Delivery of [A] dsDNA vs [B] ssDNA in response to NIR irradiation. (p<0.01, as compared to room temp + nanoshells).

These results show that overall, a higher molar concentration of ssDNA can be delivered from the composites compared to dsDNA, most likely due to the decreased size and increased flexibility of the ssDNA oligo compared to the dsDNA oligo. In addition, for both control groups, less dsDNA was delivered compared to ssDNA, as the increased size and stiffness of the dsDNA oligo also inhibited passive diffusion of the therapeutic out of the gel.

To ensure that the heating of the gel during the material transition did not denature the dsDNA oligo, the delivered product was run on a native poly(acrylamide) gel. A 20% poly(acrylamide) gel was synthesized by mixing a 19:1 molar ratio of AAm:MBAAm in tris-acetate-EDTA (TAE) buffer. The gel had a volume of ~20 ml and was polymerized by the addition of 300 μl 10% APS (w/v in H_2O) and 30 μl TEMED. The gel was loaded with a 10 bp ladder, the annealed dsDNA oligo as a positive control, and dsDNA oligo obtained from irradiating a loaded composite gel at for 30 min (808 nm, 8 W/cm^2). The gel was run at 120 V for 3 h and then stained with both SYBR gold (Invitrogen) and SYBR green (Invitrogen) by incubation of the gel with the appropriate stain for 15 min. SYBR gold stains all DNA content, while SYBR green preferentially stains dsDNA. The gel was then imaged under UV fluorescence, with the results shown in Figure 4.6.

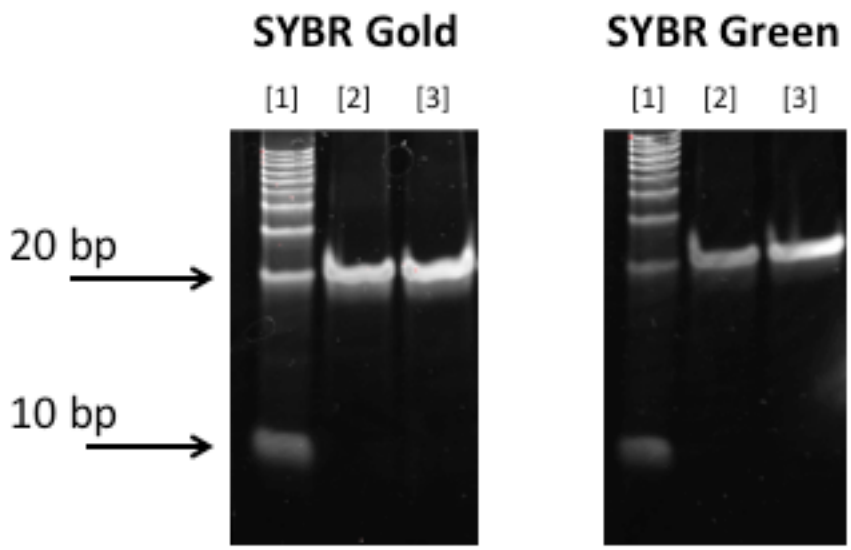

Figure 4.6. PAGE of delivered DNA. Gel electrophoresis of [1] 10 bp ladder, [2] annealed dsDNA oligo, and [3] dsDNA oligo delivered via NIR irradiation.

Results from Figure 4.6 showed that the delivered dsDNA oligo ran as a single band at 21 bp, the same size as the annealed dsDNA control. There were no bands present below the band at 21 bp, which would have indicated the presence of lower MW ssDNA. This suggests the delivered dsDNA oligo was in its double-stranded form.

4.3 CONCLUSIONS

These results validate the hypothesis that cancer therapeutics can be triggered to release from poly(NIPAAm-co-AAm)-gold nanoshell composites in response to NIR irradiation. This suggests that this material is promising for use in a remote-controlled drug delivery platform. However, for such a platform to have a strong clinical impact it must be able to be administered non-invasively. To achieve this, these composites could be synthesized as nano-scale sized particles, such that they can be injected intravenously. Chapter 5 of this thesis describes how such particles can be synthesized.

5 NANOSCALE HYDROGEL-NANOSHELL COMPOSITE SYNTHESIS AND CHARACTERIZATION

5.1 5.1 INTRODUCTION

In the previous two chapters of this thesis, a composite material for optically triggered drug delivery was synthesized and validated. The next goal is to synthesize this material as particles which are < 1 micron. These particles will be of a similar size to the nanoshells used in the studies discussed in Section 2.2.3; therefore the particles can be injected intravenously and will passively accumulate in tumor tissue due to the EPR effect. Once the particles reach the tumor site, an NIR laser will be applied to the tumor. As previously described, this will cause a rapid heating of the embedded nanoshells, which in turn triggers a collapse of the polymer coating and release of absorbed drug molecule directly at the tumor site. Figure 5.1 below illustrates this process.

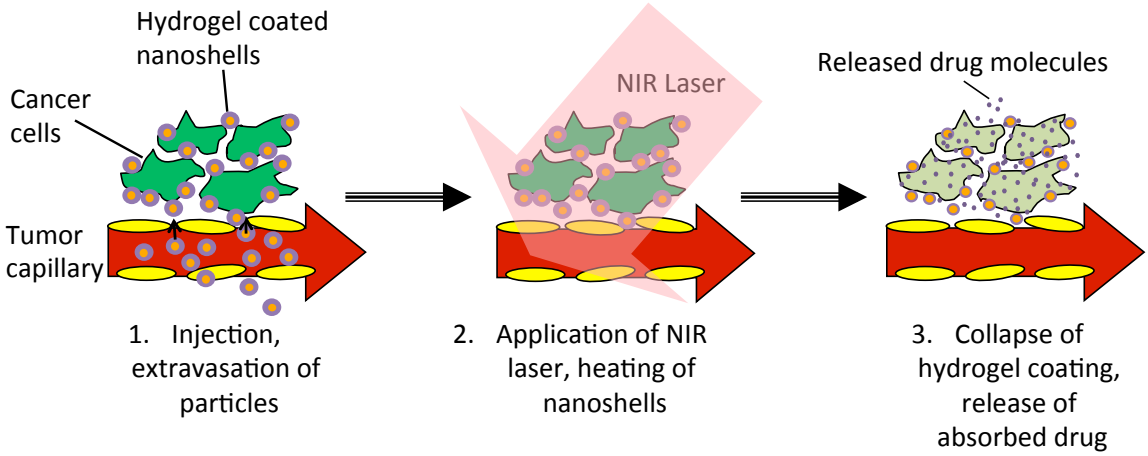

Figure 5.1. Schematic of hydrogel-nanoshell composite particle therapy. (1) Injected particles will circulate and passively accumulate into tumor tissue. (2) An applied NIR laser causes rapid heating of the embedded nanoshells. (3) The resulting temperature increase causes release of absorbed drug molecules from the thermally responsive coating directly at the tumor site.

5.2 TECHNIQUES FOR SYNTHESIS OF NANOSCALE HYDROGEL PARTICLES

In recent years, several methods have been developed to synthesize nanoscale polymer particles. Many of these methods are based on soft lithography techniques[110]. Soft lithography is generally characterized by the creation of an elastomeric stamp or mold using microfabrication techniques developed in the electronics industry[110]. Two such techniques include Particle Replication In Nonwetting Templates (PRINT)[111] and the hydrogel template method[112].

5.2.1 PRINT

The PRINT method developed by the DeSimone group uses photocurable perfluoropolyether (PFPE) molds to emboss a prepolymer solution onto a highly fluorinated surface[111]. Such surfaces are nonwetting to organic materials, thereby preventing the background "scum" layer commonly seen with traditional imprint lithography (Figure 5.2)[111].

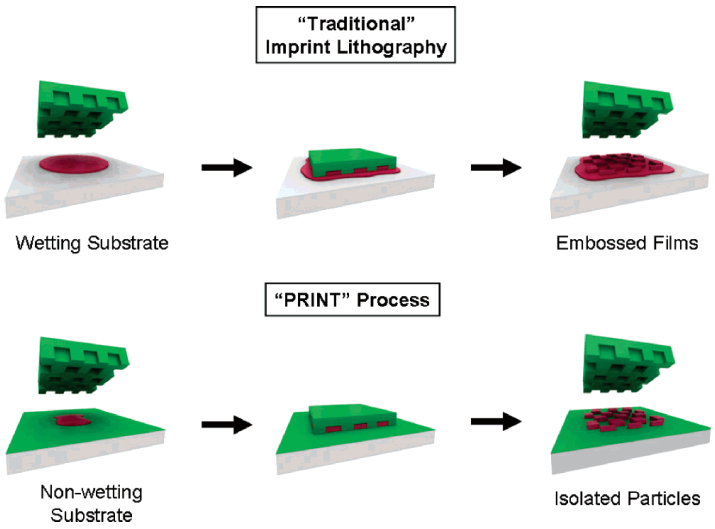

Figure 5.2. PRINT compared to traditional imprint lithography. In traditional imprint lithography, the affinity of the liquid precursor to the surface of the substrate results in a scum layer. In PRINT, the non-wetting surface causes the liquid precursor to be confined only in the wells of the mold, resulting in the synthesis of isolated particles. From Rolland *et al.* 2005[111].

This method has been used to synthesize various different particles made of materials such as poly(D-lactic acid), PEG hydrogels, and proteins; from sizes ranging from 80 nm to 20 μm[111,113]. Particles have been synthesized to be pH sensitive[114,115], and have been loaded with chemotherapeutics[114] and contrast agents[116,117].

5.2.2 Hydrogel Template Method

A novel method for synthesizing homogenous polymer particles was recently reported by the Park group[112,118]. This method relies on the use of a hydrogel template made of a material such as gelatin[112]. These gelatin templates can be easily made through common microfabrication techniques. They are mechanically stable enough to act as a mold yet undergo a sol-gel transition upon heating[112]. This process can be used to make polymer particles from 200 nm to larger than 50 μm. The hydrogel template process is summarized in Figure 5.3.

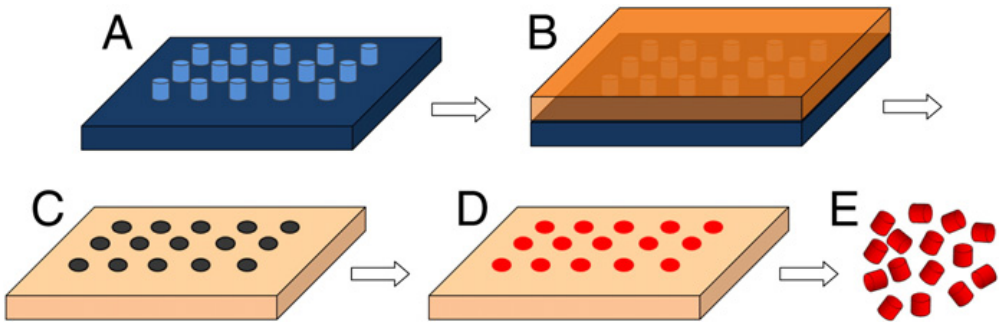

Figure 5.3. The hydrogel template method for particle synthesis. [A] A silicone wafer master is created with vertical posts of desired particle size. [B] A warm aqueous gelatin solution is poured on top of the master. [C} The gelatin is cooled to solidify and peeled off the master to expose cavities. [D] Cavities are filled with polymer mixture and dried to remove organic solvent. [E] Mold is dissolved in warm H_2O, and particles are collected by centrifugation or filtration. From Acharya *et al.* 2010[112].

An initial study examined the versatility of the synthesis method by fabricating poly(lactic-co-glycolic)acid (PLGA) particles of various sizes (from 200 nm up to 50 μm) and of various shapes, as shown in Figure 5.4[112].

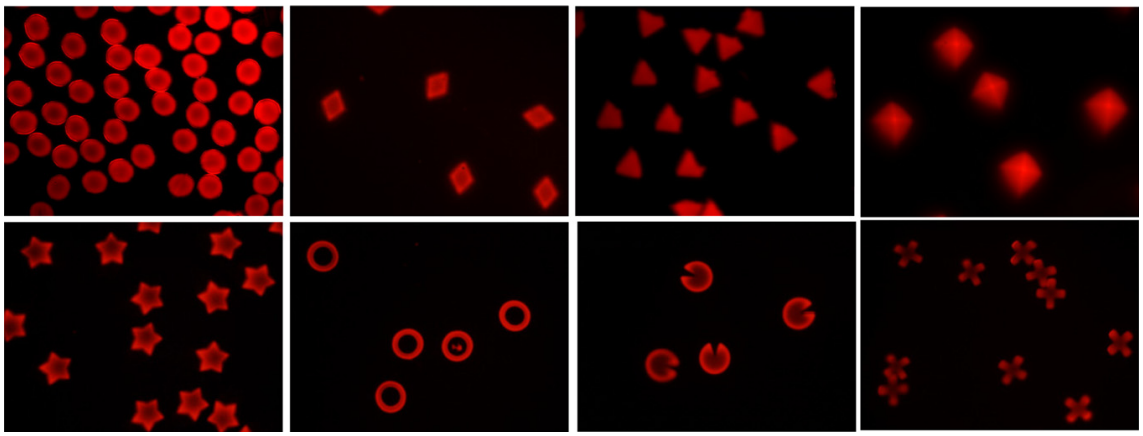

Figure 5.4. Various shapes of particles synthesized from the hydrogel template method. Particle size is 50 μm. From Acharya *et al.* 2010[112].

A further study by Acharya *et al.* analyzed drug release from degrading PLGA microparticles[118]. These particles displayed extremely high drug loading capabilities (>50% w_{drug}/w_{PLGA}) and delivered ~80-100% of loaded drug within 20-25 days. Release kinetics were dependent on surface area, diffusion coefficient, and concentration gradient[118].

5.3 HYDROGEL-NANOSHELL COMPOSITE PARTICLE SYNTHESIS

The hydrogel template method described in Section 4.2.2 was used to synthesize 500 nm poly(NIPAAm-co-AAm) hydrogels with embedded nanoshells. First, a silicone wafer master with 500 nm cylindrical (*i.e.*, 500 nm in diameter and 500 nm in height) vertical posts was created using photolithography. Each 2-inch square template contained $5x10^8$ posts. Next, 4 ml of a warmed (50-55 ^oC) 20% w/v aqueous Gelatin Type A (Sigma) solution was poured over the silicone master. After allowing the gelatin to solidify by incubating at 4^oC

for 15 min, it was peeled from the master, revealing a template with circular wells of 500 nm diameter and 500 nm height.

After template synthesis, a prepolymer solution containing NIPAAm, AAm, and MBAAm in H_2O was made as described in Section 2.2 (95:5 ratio of NIPAAm:AAm, 1:750 ratio of MBAAm:monomers). In addition, gold-silica nanoshells were added to this solution at a concentration of $1.5x10^{10}$ particles/ml. Aliquots of 100 µl were made of this prepolymer suspension, and polymerization was then initiated by addition of 2.5 µl APS (10% w/v in H_2O) and 0.5 µl TEMED. After rapid mixing by vortexing, 50 µl of this solution was pipetted onto a gelatin template and whisked across using a razor blade at a 45^o angle to completely fill the template wells. At the nanoshell concentration used, it was estimated that 1.5 nanoshells would be loaded in each well of the template. The particles were polymerized for 2 h at room temperature.

After polymerization, each template was dissolved in 10 ml H_2O (with 0.1% w/v NaN_3 to prevent microbial contamination) and incubated at 50-55^{o}C for 30-60 min. The hydrogel-nanoshell composite particles (HNCPs) were then purified by 2 rounds of centrifugation (2000xg, 5 min) and ran through a 5 µm filter. Poly(NIPAAm-co-AAm) hydrogel particles without nanoshells (NHPs) were synthesized analogously without adding nanoshells to the prepolymer solution. A schematic of this process is shown below.

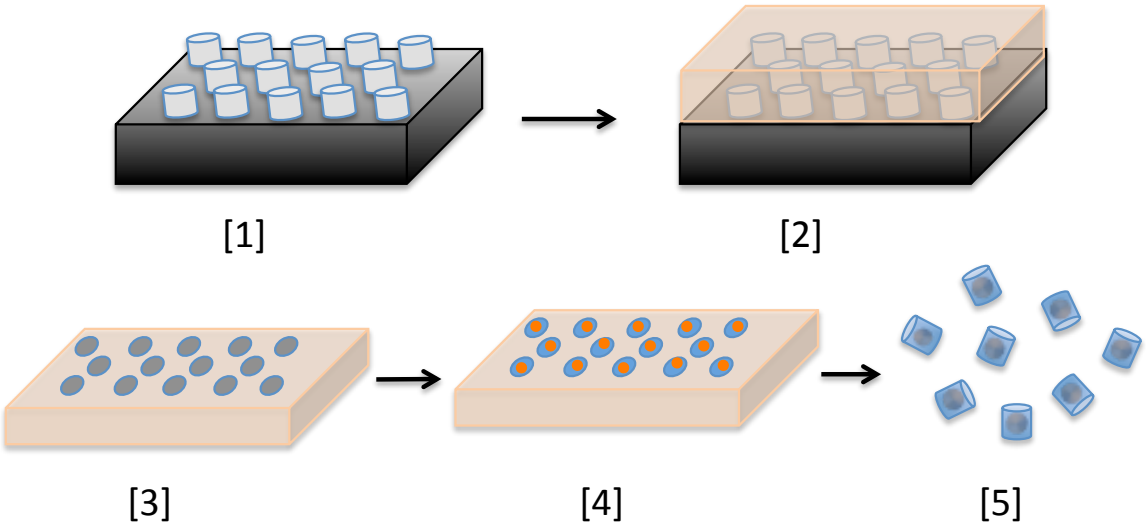

Figure 5.5. Particle synthesis based on hydrogel template method. [1] Master created with cylindrical posts 500 nm (diameter) by 500 nm (height). [2] Warm gelatin poured over master. [3] Cooled gelatin peeled off of master to reveal cavities 500 nm (diameter) by 500 nm (height). [4] Prepolymer solution and gold-silica nanoshells poured into cavities. Polymerization is initiated by APS/TEMED. [5] After polymerization, gelatin template is dissolved in warm water and HNCPs are collected by centrifugation.

5.4 Imaging Analysis

After synthesis, HNCPs were characterized using a JEOL 1230 High Contrast TEM for visual inspection of the poly(NIPAAm-co-AAm) polymer as well as any embedded gold nanoshells. Figure 5.6 shows a comparison, with the HNCPs having a thin polymer coating around the gold nanoshells. Since samples must be fully dehydrated before imaging, this coating is much smaller than it would be in its hydrated state. In addition, this drying process also provides a driving force for HNCPs to aggregate, causing many of the particles to be seen as multiple particle aggregates instead of individual particles.

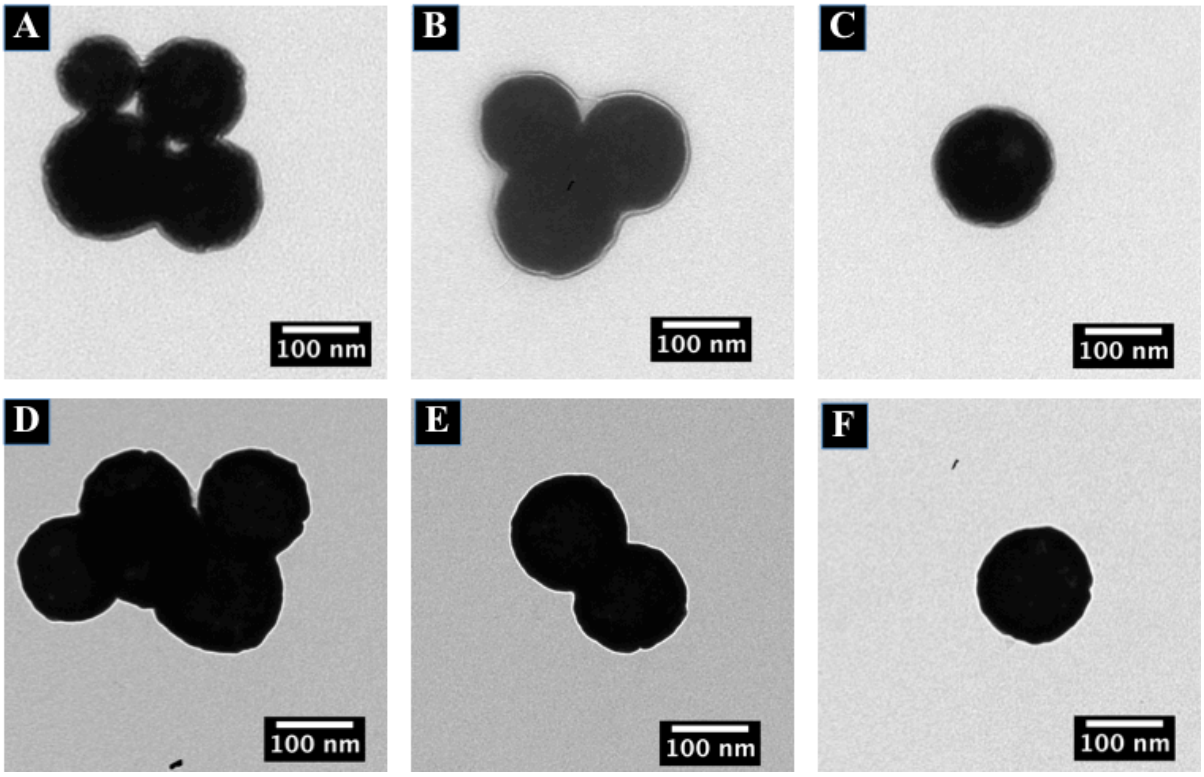

Figure 5.6. Analysis of HNCPs by TEM. [A-C] TEM images of HNCPs compared to [D-F] TEM images of bare nanoshells.

5.5 THERMAL ANALYSIS VIA DYNAMIC LIGHT SCATTERING

Dynamic light scattering (DLS) measures the Brownian motion of particles in a liquid to extrapolate their hydrodynamic radius[119]. Both HNCPs and NHPs were sized using a Brookhaven 90-Plus Particle Size Analyzer under three different conditions: at 25°C, at 50°C, and after being exposed to NIR irradiation (808 nm, 5 W/cm^2, 5 min). While this provides a technique to determine the size of sub-micron particles in a hydrated state, measurements are dependent on many factors, including the material refractive index[119]. For the NHPs, the refractive index of poly(NIPAAm) was used (1.52)[120]. However, HNCPs consist of two different materials with drastically different refractive indices. For these measurements, the refractive index of gold was used (0.169 + 3.821*i*). In addition, DLS measurements assume

particles are spherical, whereas these particles are cylindrical[119]. Due to these limitations, the hydrodynamic diameters measured are most likely not the particle's true size, so measurements for each particle type are normalized to its measurement at 25°C. The results of this study are summarized in Figure 5.7. NHPs have a significantly smaller diameter when incubated at 50°C, while the HNCPS have a significantly smaller diameter when either incubated at 50°C or exposed to NIR irradiation (as determined Student's t-test, n=3).

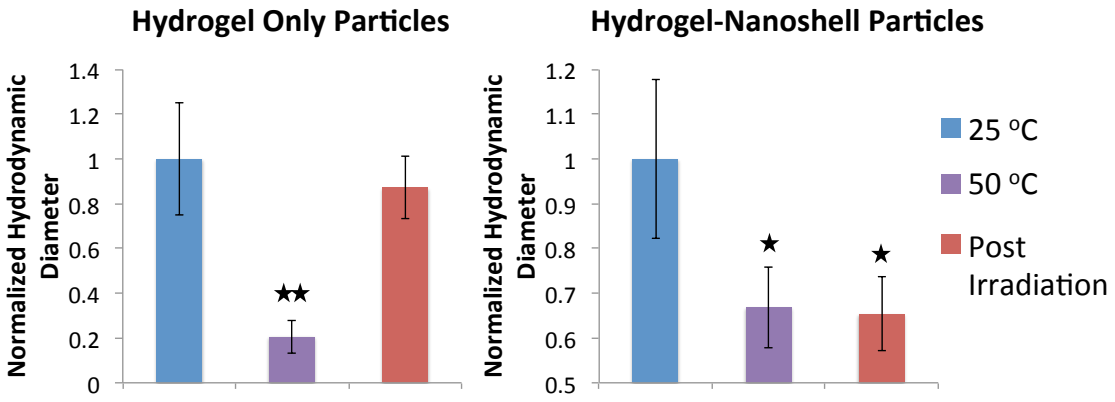

Figure 5.7. Analysis of HNCP thermal deswelling. Hydrodynamic diameters of hydrogel-only and hydrogel-nanoshell composite particles as measured by DLS. Measurements are normalized to particle size at 25°C. Hydrogel-only particles deswell in response to increased temperature, while hydrogel-nanoshell particles deswell in response to either increased temperature or exposure to NIR irradiation. (*$p<0.05$, **$p<0.01$).

Additionally, when particles were measured in their collapsed state, two separate size populations emerged, as displayed in Figure 5.8. A population at a smaller diameter represented single particles, while a second population centered around a larger diameter likely resulted from the aggregation of multiple particles. The material phase transition that causes polymer collapse will also act as a driving force for aggregation due to the hydrophobic effect. For the data displayed in Figure 5.7, only the "single particle population" of these measurements was used.

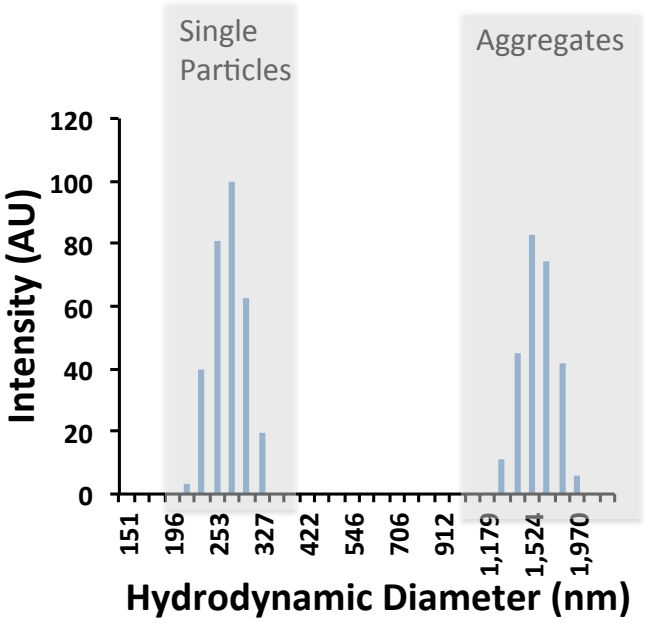

Figure 5.8. Typical size distribution of HNCPs in their collapsed stage after irradiation. The particles exhibited two distinct populations, hypothesized to be single particles vs. particle aggregates.

5.6 CONCLUSIONS

The composite material described in Chapters 3-4 was synthesized as nanoscale particles by using a dissolvable gelatin template. Image analysis using TEM indicates that the resulting particles consist of a nanoshell core surrounded by thin polymer layer. The hydrodynamic diameter of these particles decreases in response to either incubation at 50^{o}C or exposure to NIR irradiation, proving that these particles retain the same thermal properties as the bulk material. This indicates the potential of this material to be used as an injectable-sized platform for therapeutic delivery.

6 CONCLUSIONS AND FUTURE DIRECTIONS

This thesis presents work towards the creation of a novel controlled drug delivery system for cancer therapeutics. Unlike delivery systems already on the market, this platform would be administered non-invasively and allow delivery only at the site of malignant cells. Herein, the results and significance of this work will be discussed.

6.1 DEVELOPING AN OPTICALLY-TRIGGERED DELIVERY SYSTEM FOR CANCER THERAPEUTICS

The platform in this thesis was developed with two main goals in mind: (1) to encapsulate a therapeutic cargo as the platform circulated throughout the body, and (2) to trigger release of this cargo at a specific time and location.

The first goal was accomplished by the utilization of a thermally-responsive poly(NIPAAm-co-AAm) hydrogel. This material acts similarly to a sponge, allowing therapeutic molecules to be absorbed within its pores. In addition, this hydrogel was found to have an LCST of 39-45 ^{o}C, thereby existing in a swollen state at physiologic temperature.

The second goal was accomplished by the encapsulation of gold-silica nanoshells into the hydrogel. The nanoshells used in this thesis were tuned to have a peak absorption in the near-infrared range, where biological tissue is most permissive to light. When exposed to light in this range, the nanoshells heated and elicited a temperature increase of surrounding material. This caused the hydrogel material to collapse and rapidly expel large amounts of water, demonstrating the capability of optically triggering this material phase transition.

Next, it was shown that this material could be loaded with various cancer therapeutics. Both a chemotherapeutic (doxorubicin) and a biologic therapy (dsDNA, as a model for siRNA) were passively absorbed into the material, and rapid release of both therapies followed exposure to NIR irradiation. Furthermore, the heating necessary to trigger this release did not appear to detrimentally effect dsDNA integrity.

Further work was done to synthesize this composite material in the form of nanoscale particles through the use of a dissolvable gelatin template. TEM images indicated that the resulting particles consist of a nanoshell core surrounded by a hydrogel. The hydrodynamic diameter of these particles decreased in response to either incubation at 50 ^{o}C or exposure to NIR irradiation, proving that these particles retained the same thermal properties as the bulk material. This material has the potential to act as a minimally invasive delivery platform, as the nanoscale particles could be loaded with a therapeutic and injected intravenously. The platform would leak out of tumor vasculature and passively accumulate at the site of malignant tissue, at which time an external NIR laser would be used to elicit a temperature increase and release of the therapeutic payload.

6.2 FUTURE DIRECTIONS

The ability to control therapeutic delivery to malignant tissue would undoubtedly improve cancer management by overcoming limitations of current therapies. The controlled release system designed in this thesis would decrease the off-site toxicities of systemic chemotherapeutic regimens by minimizing drug exposure to non-malignant tissue, as well as increase the serum stability of fragile biologic therapeutics. The poly(NIPAAm-co-AAm)-gold nanoshell platform can be loaded with cancer therapeutics, and their release can be

optically-triggered. In addition, this material can be synthesized as sub-micron particles, giving it the potential to act as a minimally-invasive, controlled therapeutic delivery platform. Future work looking at loading and release of therapeutics from the nanoscale particles, as well as *in vitro* and *in vivo* efficacy experiments would further advance this platform. Ultimately, this single platform could also attack tumor tissue using three distinct mechanisms simultaneously: (1) photothermal heating, (2) chemotherapeutic delivery, and (3) gene silencing due to siRNA, providing a novel approach to effectively treat cancers when standard treatment modalities are not adequate.

7 REFERENCES

1. Saltiel, E. & McGuire, W. Doxorubicin (adriamycin) cardiomyopathy. *The Western journal of medicine* **139**, 332-41 (1983).

2. Oh, Y.-K. & Park, T.G. siRNA delivery systems for cancer treatment. *Advanced drug delivery reviews* **61**, 850-62 (2009).

3. Cancer Facts and Figures 2010. (2010).

4. Hanahan, D. & Weinberg, R.A. The hallmarks of cancer. *Cell* **100**, 57–70 (2000).

5. Hanahan, D. & Weinberg, R.A. Hallmarks of Cancer: The Next Generation. *Cell* **144**, 646-674 (2011).

6. McKinnell, R.G. *The Biological Basis of Cancer*. (Cambridge University Press: 1998).

7. *Clinical Oncology: A Multidisiplinary Approach for Physicians and Students*. (W.B. Saunders Company: Philadelphia, PA, 2001).

8. Seiwert, T.Y., Salama, J.K. & Vokes, E.E. The concurrent chemoradiation paradigm--general principles. *Nature clinical practice. Oncology* **4**, 86-100 (2007).

9. Bumcrot, D., Manoharan, M., Koteliansky, V. & Sah, D.W.Y. RNAi therapeutics: a potential new class of pharmaceutical drugs. *Nature chemical biology* **2**, 711-9 (2006).

10. Elbashir, S.M. *et al.* Duplexes of 21-nucleotide RNAs mediate RNA interference in cultured mammalian cells. *Nature* **411**, 494-8 (2001).

11. Controlled Drug Delivery: Challenges and Strategies. (1997).

12. Langer, R. New methods of drug delivery. *Science (New York, N.Y.)* **249**, 1527-33 (1990).

13. Langer, R.S. & Peppas, N.A. Present and future applications of biomaterials in controlled drug delivery systems. *Biomaterials* **2**, 201-14 (1981).

14. Safra, T. *et al.* Pegylated liposomal doxorubicin (doxil): reduced clinical cardiotoxicity in patients reaching or exceeding cumulative doses of 500 mg/m2. *Annals of oncology : official journal of the European Society for Medical Oncology / ESMO* **11**, 1029-33 (2000).

15. Westphal, M. *et al.* A phase 3 trial of local chemotherapy with biodegradable carmustine(BCNU) wafers (Gliadel wafers) in patients with primary malignant glioma. *Neuro-Oncology* **5**, 79-88 (2003).

16. Daniel, M.-C. & Astruc, D. Gold nanoparticles: assembly, supramolecular chemistry, quantum-size-related properties, and applications toward biology, catalysis, and nanotechnology. *Chemical reviews* **104**, 293-346 (2004).

17. Averitt, R.D., Westcott, S.L. & Halas, N.J. Ultrafast optical properties of gold nanoshells. *Journal of the Optical Society of America B* **16**, 1814 (1999).

18. Averitt, R., Sarkar, D. & Halas, N. Plasmon Resonance Shifts of Au-Coated Au2S Nanoshells: Insight into Multicomponent Nanoparticle Growth. *Physical Review Letters* **78**, 4217-4220 (1997).

19. Hirsch, L.R. *et al.* Metal nanoshells. *Annals of biomedical engineering* **34**, 15-22 (2006).

20. Yu, Y.-Y., Chang, S.-S., Lee, C.-L. & Wang, C.R.C. Gold Nanorods: Electrochemical Synthesis and Optical Properties. *The Journal of Physical Chemistry B* **101**, 6661-6664 (1997).

21. Weissleder, R. A clearer vision for in vivo imaging. *Nature Biotechnology* **19**, 316–317 (2001).

22. Turkevich, J., Stevenson, P.C. & Hillier, J. A study of the nucleation and growth processes in the synthesis of colloidal gold. *Discussions of the Faraday Society* **11**, 55 (1951).

23. Zhou, H., Honma, I., Komiyama, H. & Haus, J. Controlled synthesis and quantum-size effect in gold-coated nanparticles. *Physical Review B* **50**, 12052 (1994).

24. Gobin, A.M., Watkins, E.M., Quevedo, E., Colvin, V.L. & West, J.L. Near-infrared-resonant gold/gold sulfide nanoparticles as a photothermal cancer therapeutic agent. *Small (Weinheim an der Bergstrasse, Germany)* **6**, 745-52 (2010).

25. Averitt, R.D., Westcott, S.L. & Halas, N.J. Linear optical properties of gold nanoshells. *Journal of the Optical Society of America B* **16**, 1824 (1999).

26. Loo, C., Lowery, A., Halas, N., West, J. & Drezek, R. Immunotargeted nanoshells for integrated cancer imaging and therapy. *Nano letters* **5**, 709-11 (2005).

27. Gobin, A.M. *et al.* Near-infrared resonant nanoshells for combined optical imaging and photothermal cancer therapy. *Nano letters* **7**, 1929-34 (2007).

28. Hirsch, L., Jackson, J., Lee, A., Halas, N. & West, J. A whole blood immunoassay using gold nanoshells. *Analytical Chemistry* **75**, 2377–2381 (2003).

29. Sershen, S., Westcott, S., Halas, N. & West, J. Temperature-sensitive polymer-nanoshell composites for photothermally modulated drug delivery. *Journal of biomedical materials research* **51**, 293–298 (2000).

30. Sershen, S.R., Halas, N.J. & West, J.L. Pulsatile release of insulin via photothermally modulated drug delivery. *Proceedings of the Second Joint 24th Annual Conference and the Annual Fall Meeting of the Biomedical Engineering Society] [Engineering in Medicine and Biology* 490-491 (2002).doi:10.1109/IEMBS.2002.1136910

31. Oldenburg, S. Nanoengineering of optical resonances. *Chemical Physics Letters* **288**, 243-247 (1998).

32. Sershen, S.R., Westcott, S.L., West, J.L. & Halas, N.J. An opto-mechanical nanoshell-polymer composite. *Applied Physics B: Lasers and Optics* **73**, 379-381 (2001).

33. Sershen, S., Ng, M., Halas, N. & West, J. Optically controllable materials: Potential valves and actuators in microfluidics and MEMs. *[Engineering in Medicine and Biology, 2002. 24th Annual Conference and the Annual Fall Meeting of the Biomedical Engineering Society] EMBS/BMES Conference, 2002. Proceedings of the Second Joint* **3**, 1822–1823 (2002).

34. Sershen, S.R. *et al.* Independent Optical Control of Microfluidic Valves Formed from Optomechanically Responsive Nanocomposite Hydrogels. *Advanced Materials* **17**, 1366-1368 (2005).

35. Bikram, M., Gobin, A.M., Whitmire, R.E. & West, J.L. Temperature-sensitive hydrogels with SiO2-Au nanoshells for controlled drug delivery. *Journal of controlled release : official journal of the Controlled Release Society* **123**, 219-27 (2007).

36. Kim, J.H. & Lee, T.R. Thermo-responsive hydrogel-coated gold nanoshells for in vivo drug delivery. *Journal of Biomedical & Pharmaceutical Engineering* **2**, 29–35 (2008).

37. Mohamed, M.B., Ismail, K.Z., Link, S. & El-Sayed, M. a. Thermal Reshaping of Gold Nanorods in Micelles. *The Journal of Physical Chemistry B* **102**, 9370-9374 (1998).

38. Nikoobakht, B. & El-Sayed, M. a. Preparation and Growth Mechanism of Gold Nanorods (NRs) Using Seed-Mediated Growth Method. *Chemistry of Materials* **15**, 1957-1962 (2003).

39. Matsumura, Y. & Maeda, H. A New Concept for Macromolecular Therapeutics in Cancer Chemotherapy: Mechanism of Tumoritropic Accumulation of Proteins and the Antitumor Agent Smancs. *Cancer research* **46**, 6387 (1986).

40. Maeda, H. The enhanced permeability and retention (EPR) effect in tumor vasculature: the key role of tumor-selective macromolecular drug targeting. *Advances in enzyme regulation* **41**, 189-207 (2001).

41. Hirsch, L.R. *et al.* Nanoshell-mediated near-infrared thermal therapy of tumors under magnetic resonance guidance. *Proceedings of the National Academy of Sciences of the United States of America* **100**, 13549-54 (2003).

42. Lowery, A.R., Gobin, A.M., Day, E.S., Halas, N.J. & West, J.L. Immunonanoshells for targeted photothermal ablation of tumor cells. *International journal of nanomedicine* **1**, 149-54 (2006).

43. Bernardi, R.J., Lowery, A.R., Thompson, P. a, Blaney, S.M. & West, J.L. Immunonanoshells for targeted photothermal ablation in medulloblastoma and glioma: an in vitro evaluation using human cell lines. *Journal of neuro-oncology* **86**, 165-72 (2008).

44. Gobin, A.M., Moon, J.J. & West, J.L. EphrinA I-targeted nanoshells for photothermal ablation of prostate cancer cells. *International journal of nanomedicine* **3**, 351-8 (2008).

45. Day, E.S. *et al.* Antibody-conjugated gold-gold sulfide nanoparticles as multifunctional agents for imaging and therapy of breast cancer. *International Journal of Nanomedicine* **5**, 445 (2010).

46. O'Neal, D.P., Hirsch, L.R., Halas, N.J., Payne, J.D. & West, J.L. Photo-thermal tumor ablation in mice using near infrared-absorbing nanoparticles. *Cancer letters* **209**, 171-6 (2004).

47. Day, E.S. *et al.* Nanoshell-mediated photothermal therapy improves survival in a murine glioma model. *Journal of neuro-oncology* (2010).doi:10.1007/s11060-010-0470-8

48. James, W.D., Hirsch, L.R., West, J.L., O'Neal, P.D. & Payne, J.D. Application of INAA to the build-up and clearance of gold nanoshells in clinical studies in mice. *Journal of Radioanalytical and Nuclear Chemistry* **271**, 455-459 (2007).

49. I. Tumor Ablation Using AuroLase Therapy. (2010).

50. Galaev, I.Y. & Mattiasson, B. "Smart" polymers and what they could do in biotechnology and medicine. *Trends in biotechnology* **17**, 335–340 (1999).

51. Bikram, M. & West, J.L. Thermo-responsive systems for controlled drug delivery. *Expert opinion on drug delivery* **5**, 1077-91 (2008).

52. Chilkoti, A., Dreher, M.R., Meyer, D.E. & Raucher, D. Targeted drug delivery by thermally responsive polymers. *Advanced drug delivery reviews* **54**, 613-30 (2002).

53. Meyer, D.E., Shin, B.C., Kong, G. a, Dewhirst, M.W. & Chilkoti, a Drug targeting using thermally responsive polymers and local hyperthermia. *Journal of controlled release : official journal of the Controlled Release Society* **74**, 213-24 (2001).

54. Schild, H. Poly(N-isopropylacrylamide): experiment, theory and application. *Progress in polymer science* **17**, 163–249 (1992).

55. Sasaki, S., Kawasaki, H. & Maeda, H. Volume Phase Transition Behavior of N-Isopropylacrylamide Gels as a Function of the Chemical Potential of Water Molecules. *Macromolecules* **30**, 1847-1848 (1996).

56. Yoshida, R., Sakai, K., Okano, T. & Sakurai, Y. Modulating the phase transition temperature and thermosensitivity in N-isopropylacrylamide copolymer gels. *Journal of Biomaterials Science, Polymer Edition* **6**, 585–598 (1995).

57. Keerl, M., Smirnovas, V., Winter, R. & Richtering, W. Copolymer Microgels from Mono- and Disubstituted Acrylamides: Phase Behavior and Hydrogen Bonds. *Macromolecules* **41**, 6830-6836 (2008).

58. Owens III, D.E., Eby, J.K., Jian, Y. & Peppas, N.A. Temperature-responsive polymer–gold nanocomposites as intelligent therapeutic systems. *Journal of Biomedical Materials Research Part A* **83**, 692–695 (2007).

59. Owens, D.E. *et al.* Thermally Responsive Swelling Properties of Polyacrylamide/Poly(acrylic acid) Interpenetrating Polymer Network Nanoparticles. *Macromolecules* **40**, 7306-7310 (2007).

60. Coessens, V., Pintauer, T. & Matyjaszewski, K. Functional polymers by atom transfer radical polymerization. *Progress in Polymer Science* **26**, 337-377 (2001).

61. Odian, G.G. *Principles of Polymerization*. (Wiley-Interscience: Hoboken, NJ, 2004).

62. Barner-Kowollik, C., Quinn, J.F., Morsley, D.R. & Davis, T.P. Modeling the reversible addition-fragmentation chain transfer process in cumyl dithiobenzoate-mediated styrene homopolymerizations: Assessing rate coefficients for the addition-fragmentation equilibrium. *Journal of Polymer Science Part A: Polymer Chemistry* **39**, 1353-1365 (2001).

63. Xu, F.J., Neoh, K.G. & Kang, E.T. Bioactive surfaces and biomaterials via atom transfer radical polymerization. *Progress in Polymer Science* **34**, 719-761 (2009).

64. Urry, D.W. Physical Chemistry of Biological Free Energy Transduction As Demonstrated by Elastic Protein-Based Polymers †. *The Journal of Physical Chemistry B* **101**, 11007-11028 (1997).

65. Meyer, D.E., Kong, G.A., Dewhirst, M.W., Zalutsky, M.R. & Chilkoti, A. Targeting a Genetically Engineered Elastin-like Polypeptide to Solid Tumors by Local Hyperthermia. *Cancer research* **61**, 1548 (2001).

66. Dreher, M. Evaluation of an elastin-like polypeptide–doxorubicin conjugate for cancer therapy. *Journal of Controlled Release* **91**, 31-43 (2003).

67. Furgeson, D.Y., Dreher, M.R. & Chilkoti, A. Structural optimization of a "smart" doxorubicin-polypeptide conjugate for thermally targeted delivery to solid tumors. *Journal of controlled release : official journal of the Controlled Release Society* **110**, 362-9 (2006).

68. Liu, W. *et al.* Tumor accumulation, degradation and pharmacokinetics of elastin-like polypeptides in nude mice. *Journal of controlled release : official journal of the Controlled Release Society* **116**, 170-8 (2006).

69. Dreher, M.R., Liu, W., Michelich, C.R., Dewhirst, M.W. & Chilkoti, A. Thermal cycling enhances the accumulation of a temperature-sensitive biopolymer in solid tumors. *Cancer research* **67**, 4418-24 (2007).

70. MacKay, J.A. *et al.* Self-assembling chimeric polypeptide-doxorubicin conjugate nanoparticles that abolish tumours after a single injection. *Nature materials* **8**, 993–999 (2009).

71. Liu, W. *et al.* Injectable intratumoral depot of thermally responsive polypeptide-radionuclide conjugates delays tumor progression in a mouse model. *Journal of controlled release : official journal of the Controlled Release Society* **144**, 2-9 (2010).

72. Bidwell, G.L. & Raucher, D. Application of thermally responsive polypeptides directed against c-Myc transcriptional function for cancer therapy. *Molecular cancer therapeutics* **4**, 1076-85 (2005).

73. Satarkar, N.S. & Hilt, J.Z. Magnetic hydrogel nanocomposites for remote controlled pulsatile drug release. *Journal of controlled release : official journal of the Controlled Release Society* **130**, 246-51 (2008).

74. Satarkar, N.S., Zhang, W., Eitel, R.E. & Hilt, J.Z. Magnetic hydrogel nanocomposites as remote controlled microfluidic valves. *Lab on a chip* **9**, 1773-9 (2009).

75. Kim, J., Serpe, M.J. & Lyon, L.A. Photoswitchable microlens arrays. *Angewandte Chemie (International ed. in English)* **44**, 1333-6 (2005).

76. Wang, C., Flynn, N. T. & Langer, R. Controlled Structure and Properties of Thermoresponsive Nanoparticle–Hydrogel Composites. *Advanced Materials* **16**, 1074-1079 (2004).

77. Wang, C., Flynn, N.T. & Langer, R. Morphologically well-defined gold nanoparticles embedded in thermo-responisve hydrogel matrices. *Materials Research Society Symposium Proceedings* **820**, 1-6 (2004).

78. Frimpong, R.A., Fraser, S. & Zach Hilt, J. Synthesis and temperature response analysis of magnetic-hydrogel nanocomposites. *Journal of Biomedical Materials Research Part A* **80**, 1–6 (2007).

79. Satarkar, N.S. & Zach Hilt, J. Hydrogel nanocomposites as remote-controlled biomaterials. *Acta biomaterialia* **4**, 11-6 (2008).

80. Meenach, S. a, Anderson, a A., Suthar, M., Anderson, K.W. & Hilt, J.Z. Biocompatibility analysis of magnetic hydrogel nanocomposites based on poly(N-isopropylacrylamide) and iron oxide. *Journal of biomedical materials research. Part A* **91**, 903-9 (2009).

81. Zhao, X. *et al.* Thermoswitchable Electronic Properties of a Gold Nanoparticle/Hydrogel Composite. *Macromolecular Rapid Communications* **26**, 1784-1787 (2005).

82. Zhao, X. *et al.* A kind of smart gold nanoparticle?hydrogel composite with tunable thermo-switchable electrical properties. *New Journal of Chemistry* **30**, 915 (2006).

83. Li, J., He, W.-dong & Sun, X.-li Preperation of poly(styrene-b-N-isopropylacyrlamide) micelles surface-linked with gold nanoparticles and thermo-responsive ultraviolet-visible absorbance. *Journal of Polymer Science Part A: Polymer Chemistry* **45**, 5156-5163 (2007).

84. Kim, D.-H., Rozhkova, E. a., Rajh, T., Bader, S.D. & Novosad, V. Synthesis of Hybrid Gold/Iron Oxide Nanoparticles in Block Copolymer Micelles for Imaging, Drug Delivery, and Magnetic Hyperthermia. *IEEE Transactions on Magnetics* **45**, 4821-4824 (2009).

85. Hoare, T. *et al.* A magnetically triggered composite membrane for on-demand drug delivery. *Nano letters* **9**, 3651-7 (2009).

86. Dromi, S. *et al.* Pulsed-high intensity focused ultrasound and low temperature-sensitive liposomes for enhanced targeted drug delivery and antitumor effect. *Clinical cancer research : an official journal of the American Association for Cancer Research* **13**, 2722-7 (2007).

87. Qin, G. *et al.* Partially polymerized liposomes: stable against leakage yet capable of instantaneous release for remote controlled drug delivery. *Nanotechnology* **22**, 155605 (2011).

88. Agarwal, A., Mackey, M.A., El-Sayed, M.A. & Bellamkonda, R.V. Remote triggered release of doxorubicin in tumors by synergistic application of thermosensitive liposomes and gold nanorods. *ACS nano* **5**, 4919-26 (2011).

89. Shan, J., Chen, J., Nuopponen, M. & Tenhu, H. Two phase transitions of poly(N-isopropylacrylamide) brushes bound to gold nanoparticles. *Langmuir : the ACS journal of surfaces and colloids* **20**, 4671-6 (2004).

90. Shan, J. *et al.* Amphiphilic Gold Nanoparticles Grafted with Poly(N -isopropylacrylamide) and Polystyrene. *Macromolecules* **38**, 2918-2926 (2005).

91. Nuopponen, M. & Tenhu, H. Gold nanoparticles protected with pH and temperature-sensitive diblock copolymers. *Langmuir : the ACS journal of surfaces and colloids* **23**, 5352-7 (2007).

92. Yusa, S.-ichi *et al.* Salt effect on the heat-induced association behavior of gold nanoparticles coated with poly(N-isopropylacrylamide) prepared via reversible addition-fragmentation chain transfer (RAFT) radical polymerization. *Langmuir : the ACS journal of surfaces and colloids* **23**, 12842-8 (2007).

93. Kim, J.H. & Randall Lee, T. Discrete Thermally Responsive Hydrogel-coated gold Nanoparticles for Use as Drug-Delivery Vehicles. *Drug development research* **67**, 61–69 (2006).

94. Kim, J.-H. & Lee, T.R. Hydrogel-templated growth of large gold nanoparticles: synthesis of thermally responsive hydrogel-nanoparticle composites. *Langmuir : the ACS journal of surfaces and colloids* **23**, 6504-9 (2007).

95. Frimpong, R. a & Hilt, J.Z. Poly(n-isopropylacrylamide)-based hydrogel coatings on magnetite nanoparticles via atom transfer radical polymerization. *Nanotechnology* **19**, 175101 (2008).

96. Wei, Q., Ji, J. & Shen, J. Synthesis of Near-Infrared Responsive Gold Nanorod/PNIPAAm Core/Shell Nanohybrids via Surface Initiated ATRP for Smart Drug Delivery. *Macromolecular Rapid Communications* **29**, 645-650 (2008).

97. Chakraborty, S., Bishnoi, S.W. & Pérez-Luna, V.H. Gold Nanoparticles with Poly(N -isopropylacrylamide) Formed via Surface Initiated Atom Transfer Free Radical Polymerization Exhibit Unusually Slow Aggregation Kinetics. *The Journal of Physical Chemistry C* **114**, 5947-5955 (2010).

98. Singh, N. & Lyon, L.A. Au Nanoparticle Templated Synthesis of pNIPAm Nanogels. *Chemistry of Materials* **19**, 719-726 (2007).

99. Morones, J.R. & Frey, W. Room temperature synthesis of an optically and thermally responsive hybrid PNIPAM-gold nanoparticle. *Journal of Nanoparticle Research* **12**, 1401–1414 (2010).

100. Huang, H.-C. *et al.* Optically Responsive Gold Nanorod−Polypeptide Assemblies. *Langmuir* **24**, 14139-14144 (2008).

101. STOBER, W. Controlled growth of monodisperse silica spheres in the micron size range*1. *Journal of Colloid and Interface Science* **26**, 62-69 (1968).

102. Duff, D.G., Baiker, A. & Edwards, P.P. A new hydrosol of gold clusters. 1. Formation and particle size variation. *Langmuir* **9**, 2301-2309 (1993).

103. Karukstis, K.K., Thompson, E.H.., Whiles, J.A. & Rosenfeld, R.J. Deciphering the fluorescence signature of daunomycin and doxorubicin. *Biophysical Chemistry* **73**, 249-263 (1998).

104. Arcamone, F. *et al.* Adriamycin, 14-hydroxydaunomycin, a new antitumor antibiotic from S. peucetius var. caesius. *Biotechnology and bioengineering* **11**, 1101-10 (1969).

105. Fornari, F.A., Randolph, J.K., Yalowich, J.C., Ritke, M.K. & Gewirtz, D.A. Interference by doxorubicin with DNA unwinding in MCF-7 breast tumor cells. *Molecular pharmacology* **45**, 649-56 (1994).

106. Gale, N.W. & Yancopoulos, G.D. Growth factors acting via endothelial cell-specific receptor tyrosine kinases: VEGFs, angiopoietins, and ephrins in vascular development. *Genes & development* **13**, 1055-66 (1999).

107. Landen, C.N. *et al.* Therapeutic EphA2 gene targeting in vivo using neutral liposomal small interfering RNA delivery. *Cancer research* **65**, 6910-8 (2005).

108. Smith, S.B., Cui, Y. & Bustamante, C. Overstretching B-DNA: The Elastic Response of Individual Double-Stranded and Single-Stranded DNA Molecules. *Science* **271**, 795-799 (1996).

109. Bustamante, C., Smith, S.B., Liphardt, J. & Smith, D. Single-molecule studies of DNA mechanics. *Current Opinion in Structural Biology* **10**, 279-285 (2000).

110. Jeong, W., Napier, M.E. & DeSimone, J.M. Challenging nature's monopoly on the creation of well-defined nanoparticles. *Nanomedicine (London, England)* **5**, 633-9 (2010).

111. Rolland, J.P. *et al.* Direct fabrication and harvesting of monodisperse, shape-specific nanobiomaterials. *Journal of the American Chemical Society* **127**, 10096-100 (2005).

112. Acharya, G. *et al.* The hydrogel template method for fabrication of homogeneous nano/microparticles. *Journal of controlled release : official journal of the Controlled Release Society* **141**, 314-9 (2010).

113. Kelly, J.Y. & DeSimone, J.M. Shape-specific, monodisperse nano-molding of protein particles. *Journal of the American Chemical Society* **130**, 5438-9 (2008).

114. Petros, R.A., Ropp, P.A. & DeSimone, J.M. Reductively labile PRINT particles for the delivery of doxorubicin to HeLa cells. *Journal of the American Chemical Society* **130**, 5008-9 (2008).

115. Parrott, M.C. *et al.* Tunable bifunctional silyl ether cross-linkers for the design of acid-sensitive biomaterials. *Journal of the American Chemical Society* **132**, 17928-32 (2010).

116. Parrott, M.C. *et al.* Incorporation and Controlled Release of Silyl Ether Prodrugs from PRINT Nanoparticles. *Journal of the American Chemical Society* 120423200814002 (2012).doi:10.1021/ja301710z

117. Nunes, J., Herlihy, K.P., Mair, L., Superfine, R. & DeSimone, J.M. Multifunctional shape and size specific magneto-polymer composite particles. *Nano letters* **10**, 1113-9 (2010).

118. Acharya, G. *et al.* A study of drug release from homogeneous PLGA microstructures. *Journal of controlled release : official journal of the Controlled Release Society* **146**, 201-6 (2010).

119. Malvern Instruments Ltd Dynamic Light Scattering: An Introduction in 30 Minutes. doi:MRK656-01

120. Reufer, M., Díaz-Leyva, P., Lynch, I. & Scheffold, F. Temperature-sensitive poly(N-isopropyl-acrylamide) microgel particles: a light scattering study. *The European physical journal. E, Soft matter* **28**, 165-71 (2009).